Advances in Materials Science and Engineering

Photocatalytic Materials

Guest Editors: Guohua Jiang, Tao Chen, and Qiang Yang

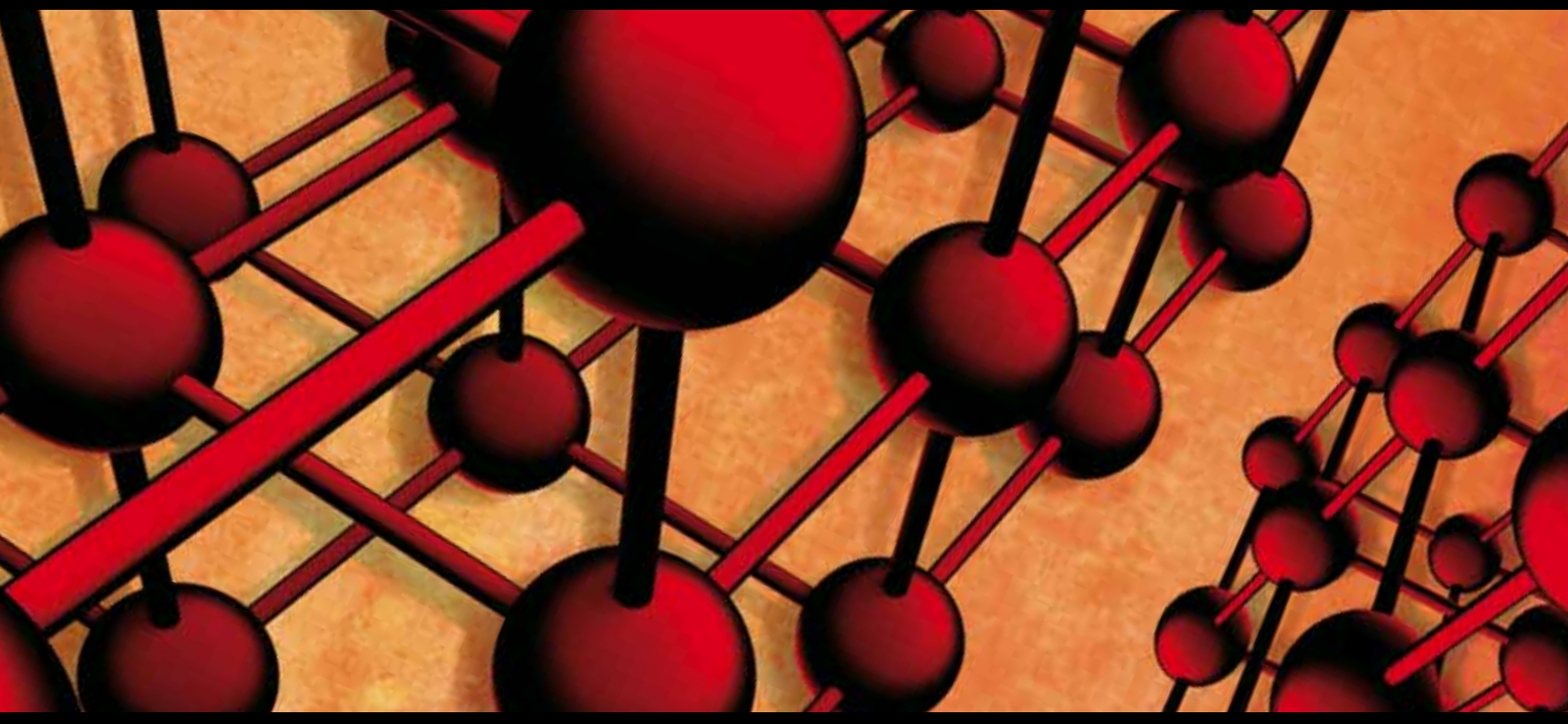

Photocatalytic Materials

Advances in Materials Science and Engineering

Photocatalytic Materials

Guest Editors: Guohua Jiang, Tao Chen, and Qiang Yang

Editorial Board

Contents

Photocatalytic Materials, Guohua Jiang, Tao Chen, and Qiang Yang
Volume 2012, Article ID 186948, 2 pages

Photocatalytic Degradation of Dichlorvos in Visible Light by Mg^{2+}-TiO_2 Nanocatalyst, T. Siva Rao, Teshome Abdo Segne, T. Susmitha, A. Balaram Kiran, and C. Subrahmanyam
Volume 2012, Article ID 168780, 9 pages

Optimization of Nano-TiO_2 Photocatalytic Reactor for Organophosphorus Degradation, Ilin Sadeghi, Pooya Arbab, Mahdi Fathizadeh, Hoseen Fakhraee, and Mahdi Amrollahi
Volume 2012, Article ID 510123, 5 pages

Photocatalytic Properties of Columnar Nanostructured TiO_2 Films Fabricated by Sputtering Ti and Subsequent Annealing, Zhengcao Li, Liping Xing, and Zhengjun Zhang
Volume 2012, Article ID 413638, 5 pages

Preparation and Photocatalytic Activity of Magnetic $Fe_3O_4/SiO_2/TiO_2$ Composites, Rijing Wang, Xiaohong Wang, Xiaoguang Xi, Ruanbing Hu, and Guohua Jiang
Volume 2012, Article ID 409379, 8 pages

Synthesis and Characterization of Fe-N-S-tri-Doped TiO_2 Photocatalyst and Its Enhanced Visible Light Photocatalytic Activity, Biying Li, Xiuwen Cheng, Xiujuan Yu, Lei Yan, and Zipeng Xing
Volume 2012, Article ID 348927, 5 pages

Hindawi Publishing Corporation
Advances in Materials Science and Engineering
Volume 2012, Article ID 186948, 2 pages
doi:10.1155/2012/186948

Editorial

Photocatalytic Materials

Guohua Jiang,[1] Tao Chen,[2] and Qiang Yang[3]

[1] *Department of Materials Engineering, College of Materials and Textile, Zhejiang Sci-Tech University, Hangzhou 310018, China*
[2] *Division of Polymer and Composite, Ningbo Institute of Materials Technology and Engineering, Chinese Academy of Sciences, Ningbo 315201, China*
[3] *Department of Biological Systems Engineering, University of Wisconsin-Madison, Madison 53706, USA*

Correspondence should be addressed to Guohua Jiang, polymer_jiang@hotmail.com

Received 13 December 2012; Accepted 13 December 2012

With the rapid development of global industry, steadily worsening environmental pollution and energy shortages have raised awareness of a potential global crisis. So it is urgent to develop a simple and effective method to address these current issues. In recent years, semiconductor photocatalysis has emerged as one of the most promising technologies because it represents an easy way to utilize the energy of either natural sunlight or artificial indoor illumination and is thus abundantly available everywhere in the world. The potential applications of photocatalysis are found mainly in the following fields: (i) photolysis of water to yield hydrogen fuel; (ii) photodecomposition or photooxidization of hazardous substances; (iii) artificial photosynthesis; (iv) photoinduced superhydrophilicity; (v) photoelectrochemical conversion, and so forth [1].

Among various common photocatalysts, bits photocatalytic activity under UVTiO_2 has been extensively used in a wide range of applications (such as gas sensor, solar cell, batteries, etc.), since the discovery of its application in photocatalysis [2]. Since then, intense research has been carried out on TiO_2 photocatalysis, which has been focused on understanding the fundamental principles, enhancing the photocatalytic efficiency, and expanding the scope of applications. Many potential uses of TiO_2 photocatalysis have been identified, such as the hydrogen fuel production, detoxification of effluents, disinfection, superhydrophilic self-cleaning, the elimination of inorganic/organic gaseous pollutants, and the synthesis of organic fuels.

To further improve the photocatalytic performance, there has been great interest in preparation of the supported nanocatalysts, for instance, carbon nanotubes composites, magnetic composites, graphene composites, and so forth, because of their enhanced photocatalytic activity or magnetic separation [3]. Nanomaterials have emerged as pioneering photocatalysts and account for most of the current research in this area. Nanomaterials can provide large surface areas, diverse morphologies, abundant surface states, and easy device modeling, all of which are properties beneficial to photocatalysis. Significant progress has been made in the development of novel nanomaterials in recent years. Nevertheless, the efficiency of nanomaterials, especially in solar photocatalysis, must be improved in order to meet engineering requirements. For example, TiO_2 exhibits photocatalytic activity under UV light ($\lambda < 387$ nm), whose energy exceeds its band gap, resulting in its limited practical applications [4–6]. Therefore, the exploitation of visible-light-driven photocatalysts is indispensable for the practical application of the photocatalytic system. Furthermore, the stability and cost of these materials should also be carefully considered. It is thus a challenge of great importance to identify and design new semiconductor materials that are efficient, stable, and abundant.

Another key issue influencing the photocatalytic capability of a semiconductor is the nature of its surface/interface chemistry. The surface energy and chemisorption properties play crucial roles in the transfer of electrons and energy between substances at the interface, in governing the selectivity, rate, and overpotential of redox reactions on the photocatalyst surface, and in determining the susceptibility of the photocatalyst toward photocorrosion [1]. In general, a higher surface energy yields higher catalytic activity. Recently, much interest has been focused on research into semiconductor crystals with morphologies, such as nanorods, nanoparticles, nanotubes, and micro/nanospheres, which have been

fabricated successfully and that provide large percentages of highly reactive facets [7–10]. Appropriate modification of the surface is frequently necessary to facilitate photocatalysis.

Despite important insight being gained, the mechanisms involved in photocatalysis are not yet known in detail. Fulfilling this goal requires the help of theoretical investigations such as electronic structure calculations and molecular dynamic simulations. Indeed, the theoretical study of photocatalysis has progressed rapidly alongside the experimental work. The above computational methods require a degree of understanding of photocatalysis. The calculation results obtained then raise the level of this understanding and provide guidance toward the practical improvement of photocatalytic materials and their applications.

The papers in this special issue concern the development of new photocatalytic nanomaterials for degradation of organic pollutes. They concentrate on preparation of photocatalytic materials, with assistant of magnetic nanoparticles, metal or nonmetal doping, annealing treatment. Novel photocatalytic materials or special preparation process are provided to solve limited photocatalytic activity that hindered by the lack of visible absorption. The works assembled in the present volume contribute to such development. Hopefully, they will inspire further research along the same lines.

Acknowledgments

We would like to thank all authors who have submitted their manuscripts to this special issue and the following external reviewers for their invaluable contributions to the reviewing process: Haojie Yu, Wenqin Wang, Jiaguo Yu, Yin Wang, Xinke Sun, Panayota G. Vassiliou, Jia Huo. We would like to thank Hindawi Publishing Corporation for giving us this great opportunity of organizing this special issue.

Guohua Jiang
Tao Chen
Qiang Yang

References

[1] H. Tong, S. Ouyang, Y. Bi, N. Umezawa, M. Oshikiri, and J. Ye, "Nano-photocatalytic materials: possibilities and challenges," *Advanced Materials*, vol. 24, pp. 229–251, 2012.

[2] A. Fujishima and K. Honda, "Electrochemical photolysis of water at a semiconductor electrode," *Nature*, vol. 238, no. 5358, pp. 37–38, 1972.

[3] R. Wang, G. Jiang, Y. Ding et al., "Photocatalytic activity of heterostructures based on TiO_2 and halloysite nanotubes," *ACS Applied Materials & Interfaces*, vol. 3, pp. 4154–4158, 2011.

[4] S. Yin, B. Liu, P. Zhang, T. Morikawa, K. I. Yamanaka, and T. Sato, "Photocatalytic oxidation of NOx under visible led light irradiation over nitrogen-doped titania particles with iron or platinum loading," *Journal of Physical Chemistry C*, vol. 112, no. 32, pp. 12425–12431, 2008.

[5] Y. Ide, M. Matsuoka, and M. Ogawa, "Efficient visible-light-induced photocatalytic activity on gold-nanoparticle-supported layered titanate," *Journal of the American Chemical Society*, vol. 132, no. 47, pp. 16762–16764, 2010.

[6] G. Jiang, R. Wang, H. Jin et al., "Preparation of Cu_2O/TiO_2 composite porous carbon microspheres as efficient visible light-responsive photocatalysts," *Powder Technology*, vol. 212, no. 1, pp. 284–288, 2011.

[7] G. Jiang, X. Wang, Y. Zhou et al., "Hollow TiO_2 nanocages with Rubik-like structure for high-performance photocatalysts," *Materials Letters*, vol. 89, pp. 59–62, 2012.

[8] G. Jiang, R. Wang, X. Wang et al., "Novel highly active visible-light-induced photocatalysts based on BiOBr with Ti doping and Ag decorating," *ACS Applied Materials & Interfaces*, vol. 4, pp. 4440–4444, 2012.

[9] D. Jian, P. X. Gao, W. Cai et al., "Synthesis, characterization, and photocatalytic properties of $ZnO/(La,Sr)CoO_3$ composite nanorod arrays," *Journal of Materials Chemistry*, vol. 19, no. 7, pp. 970–975, 2009.

[10] J. Huang, K. Ding, Y. Hou, X. Wang, and X. Fu, "Synthesis and photocatalytic activity of Zn_2GeO_4 nanorods for the degradation of organic pollutants in water," *ChemSusChem*, vol. 1, no. 12, pp. 1011–1019, 2008.

Hindawi Publishing Corporation
Advances in Materials Science and Engineering
Volume 2012, Article ID 168780, 9 pages
doi:10.1155/2012/168780

Research Article

Photocatalytic Degradation of Dichlorvos in Visible Light by Mg^{2+}-TiO_2 Nanocatalyst

T. Siva Rao,[1] Teshome Abdo Segne,[1] T. Susmitha,[1] A. Balaram Kiran,[1] and C. Subrahmanyam[2]

[1] *Department of Inorganic and Analytical Chemistry, School of Chemistry, Andhra University, Visakhapatnam 530003, India*
[2] *Department of Chemistry, Indian Institute of Technology Hyderabad, Hyderabad 500007, India*

Correspondence should be addressed to T. Siva Rao, raost@yahoo.com

Received 30 January 2012; Revised 8 March 2012; Accepted 19 March 2012

Academic Editor: Guohua Jiang

Photocatalytic activity of TiO_2 was studied by doping with magnesium (Mg^{2+}-TiO_2) with varying magnesium weight percentages ranging from 0.75–1.5 wt%. The doped and undoped samples were synthesized by sol-gel method and characterized by X-ray diffraction (XRD), N_2 adsorption-desorption (BET), X-ray photoelectron spectroscopy (XPS), UV-visible diffuse reflectance spectroscopy (DRS), and scanning electron microscopy (SEM). The XRD data has shown that anatase crystalline phase in Mg^{2+}-TiO_2 catalysts, indicating that Mg^{2+} ions did not influence the crystal patterns of TiO_2. The presence of magnesium ions in TiO_2 matrix has been determined by XPS spectra. DRS spectra showed that there is a significant absorption shift towards the visible region for doped TiO_2. The SEM images and BET results showed that doped catalyst has smaller particle size and highest surface area than undoped TiO_2. The photocatalytic efficiency of the synthesized catalysts was investigated by the photocatalytic degradation of aqueous dichlorvos (DDVP) under visible light irradiation, and it was found that the Mg^{2+}-doped catalysts have better catalytic activity than undoped TiO_2. This can be attributed that there is a more efficient electron-hole creation in Mg^{2+}-TiO_2 in visible light, contrary to undoped TiO_2 which can be excited only in UV irradiation. The effect of dopant concentration, pH of solution, dosage of catalysts, and initial pesticide concentration has been studied.

1. Introduction

Advanced oxidation process (AOP) is an alternative way of treating undesirable organic pollutants, including pesticides. According to the literature [1, 2] among AOPs, heterogeneous photocatalysis seems to be an attractive method and has been successfully employed for the degradation or transform into less harmful substances of various families of pollutants [3–5].

The photoinduced redox reactions have received an attention after the discovery of first photoelectrochemical splitting of water on titanium dioxide electrode by Fujishima and Honda [6]. Later, many novel redox reactions of organic and inorganic substrates have been induced by band-gap irradiation of a variety of semiconductor particles [7, 8]. There are a lot of different semiconductor materials which are readily available (e.g., TiO_2, ZnO, Fe_2O_3, CdS, and ZnS), but only a few are suitable for sensitizing the photomineralization of a wide range of organic pollutants. A sensitizer for reaction must be [9, 10] (i) photoactive, (ii) able to utilize visible and/or near the UV light, (iii) biologically and chemically inert, and (iv) photostable.

Among various semiconductor photocatalysts available, TiO_2 has attracted a great deal of study for its high photocatalytic activity, nontoxic property, chemical stability, and highest oxidation rate of many photoactive metal oxides investigated [11]. TiO_2 is capable of decomposing a wide range of organic, inorganic, and toxic pollutants [12].

Although TiO_2 is superior to other semiconductors for many practical uses, two types of defects limit its photocatalytic activity. Firstly, TiO_2 has high bandgap energy (3.2 eV), which is only 4-5% of the overall solar spectrum. Thus this restricts the use of visible light. Secondly, the high rate of electron-hole recombination at TiO_2 particles results in low photoquantum efficiency [13]. In order to overcome these limitations of TiO_2, many attempts have been made to prepare different types of TiO_2 by depositing of noble metals, mixing metal oxides, surface derivatization, and doping

selective metal ions into TiO_2 [14, 15], and also Graphene-based semiconductor photocatalysts are prepared [16].

The addition of low percentage of metal by doping was often proposed to improve the photocatalytic activity of TiO_2. The advantage of doping the metal ions into TiO_2 is the temporary trapping of the photogenerated charge carriers by the dopant and the inhibition of their recombination during migration from the inside of the material to the surface, by modifying the bandgap of the photocatalyst. A wide range of metal ions have been studied for doping TiO_2 and their effects on the properties of TiO_2 and on its photocatalysis [17, 18], but reports on alkaline-earth metal ions doping into TiO_2 and their photocatalytic properties have seldom been seen.

Sol-gel process is one of the versatile, simple, and easy means of synthesizing nanosize materials in contrast to the other conventional preparation methods which do not usually produce homogeneous, high-surface-area materials. The main advantage of the sol-gel method in preparing catalytic materials is its excellent control over the properties of the product via a host of parameters that are accessible in all four key processing steps: formation of a gel, aging, drying, and heat treatment. Although titania catalysts have been extensively studied, the procedure of preparing photocatalytic metal-doped titania is still of great interest.

Waste waters generated from the agricultural application of dichlorvos contain the residue of dichlorvos which has been evaluated in a wide range of toxicology assays including bioassays for carcinogenicity and mutagenicity (genotoxicity) [19, 20]. It is also more likely to contaminate surface and ground waters due to its high solubility in water. This could have an adverse effect on the aquatic environment, and procedure has to be found for its degradation. Electron transfer process occurring between pesticide and semiconductor, especially TiO_2, has been examined and found to have practical potential [21].

The present paper has been focused to develop a visible light response catalyst via magnesium-doped titanium dioxide in varying percentages of metal. Characterization has been carried out using XRD, BET, XPS, DRS, and SEM. The photocatalytic activities of the synthesized samples have been evaluated by the degradation of a representative model pesticide pollutant, dichlorvos.

2. Experimental

2.1. Preparation of Photocatalysts. Titanium tetra-n-butoxide [$Ti(O\text{-}Bu)_4$] and magnesium nitrate were obtained from E. Merck (Germany) and used as titanium and magnesium sources for preparing anatase TiO_2 and Mg^{2+}-TiO_2 photo catalysts. Aqueous dichlorvos solution was used as a model compound for degradation. All other chemicals used in this work are of analytical grade, and doubly distilled water was used for the solution preparation.

Mg^{2+}-TiO_2 samples were prepared by sol-gel method in which initially a solution containing 40 mL of absolute alcohol, 6 mL of H_2O, and magnesium nitrate with required percentages (0.75 wt.%, 1.00 wt.%, 1.25 wt.% and 1.50 wt.%) was prepared (solution I). Another solution was prepared by taking 21 mL of $Ti(O\text{-}Bu)_4$ in 40 mL of absolute alcohol with stirring for 10 minutes, and then 3 mL of HNO_3 was added dropwise under continuous stirring for 30 minutes (solution II). Solution I was added to solution II slowly from the burette with vigorous stirring at room temperature until the transparent sol was obtained, and the resulting sol was further stirred for 1 h. The gel was prepared by aging the solution for 48 h at room temperature. The derived gel was dried at 100°C in an oven and ground. The catalyst powder was calcined at 400°C in furnace for 2 h. Undoped TiO_2 is also prepared with same procedure without metal nitrate. The doping concentrations are expressed as weight percentage of titanium atom. The powders are stored in black coated air-tight glass containers.

2.2. Characterization of Photocatalysts. The crystal phase composition of the prepared photocatalysts (TiO_2, Mg^{2+}-TiO_2) was determined by X-ray diffraction measurement carried out at room temperature using a PANalytical, D/Max-III A diffractometer with CuK_α radiation (λ = 0.15148 nm) with a liquid nitrogen gas-cooled germanium solid-state detector. The accelerating voltage of 35 kV and emission current of 30 mA were used and studied in the range of 2°–90° 2θ with a step time of 2° min^{-1}. The Brunauer-Emmett-Teller (BET) surface area was determined from the N_2 adsorption-desorption isotherm at 77.3 K by using a Quantachrome Nova 2200 E system. The sample was outgassed for 3 h at 300°C prior to the adsorption. The specific surface area was determined by using the standard BET method. To study the valence state of the photocatalysts, X-ray photoelectron spectroscopy (XPS) was recorded with the PHI quantum ESCA microprobe system, using the AlK_α line of a 250 W X-ray tube as a radiation source with the energy of 1486.6 eV, 16 mA × 12.5 kV, and a working pressure lower than 1×10^{-8} Nm^{-2}. As an internal reference for the absolute binding energies, the C 1s peak of hydrocarbon contamination was used as reference to 284.8 eV. The fitting of XPS curves was analyzed with MultiPak 6.0 A software. The DRS were recorded with a Shimadzu 3600 UV-visible NIR spectrophotometer equipped with an integrating sphere diffuse reflectance accessory, using $BaSO_4$ as reference scatter. Powder samples were loaded into a quartz cell, and spectra were recorded in the range of 200–900 nm. The morphology and size of particles was characterized using SEM (JSM-6610 LV) spectrophotometer and operated at 20 kV. A Horiba Jobin FluoroMax-4 instrument has been used for the PL, spectral data analysis, with a PMT voltage was 150 V and with slit set both at 2.5 nm.

2.3. Photocatalytic Activity of the Catalysts. Photocatalytic degradation studies of DDVP were carried out in a modified photoreactor system, in which 100 mL of reaction mixture illuminated with 400 W high-pressure mercury vapor lamp (Osram, India). The distance between the light source and the reaction beaker was 20 cm. Prior to irradiation, the solution with catalyst was stirred in the dark for 45 min to ensure establishment of adsorption-desorption equilibrium

of dichlorvos on catalyst surface. Aliquots of the samples were withdrawn from the solution by using Millipore syringe (0.45 μm) at certain time intervals and analyzed for dichlorvos concentration. The quantitative determination of DDVP was performed by measuring the absorption of phosphate ion formed at 465 nm with a Milton-Roy spectronic-1201 UV-visible spectrometer. The IR (>700 nm) and UV (<360 nm) radiations were filtered by water and UV filters, respectively.

Previous studies have shown that the photocatalytic degradation of pesticides by irradiating with UV light source and using TiO_2 or ZnO as catalyst leads to the formation of H^+, Cl^-, PO_4^{3-}, and CO_2 as final products, and their formation during the progress of the degradation of DDVP was confirmed by simple qualitative analysis tests. PO_4^{3-} was determined calorimetrically by the molybdenum blue method:

$$(CH_3O)_2POOCHCCl_2 + \left(\frac{9}{2}\right)O_2 \longrightarrow PO_4^{3-} + 4CO_2 + 2\ Cl^- + 5\ H^+ + H_2O. \quad (1)$$

Hence, in order to study the extent of mineralization of DDVP over illuminated Mg^{2+}-doped TiO_2, the absorbance measurements of PO_4^{3-} were carried out. The percentage of degradation was calculated from the following equation:

$$\%\ \text{Phosphate ion formation} = \left[\frac{A_t}{A_0}\right] \times 100, \quad (2)$$

where A_0 is calculated concentration of phosphate ion of the corresponding concentration and A_t is absorbance at time t.

3. Results and Discussions

3.1. XRD Diffraction Study and BET Results. The crystalline phases of the synthesized TiO_2 and Mg^{2+}-TiO_2 were examined by XRD, and the diffractograms are given in Figure 1. The XRD patterns of calcined (400°C) TiO_2 and the samples of Mg^{2+}-TiO_2 (Mg/Ti = 0.75, 1.0 and 1.25 wt.%) show only anatase form, indicating that Mg^{2+} ions in TiO_2 did not influence the crystal patterns of TiO_2 particle. Further, examination of XRD patterns of both pure and Mg^{2+}-doped TiO_2 illustrates the existence of peaks at 25.3, 37.7, 47.7, and 54.2 (2θ). The intensity of anatase TiO_2 peaks increased due to doping, and peaks corresponding to $MgNO_3$ and $MgCO_3$ were not detected. This may be due to the well dispersion of Mg^{2+} content in TiO_2 particles.

Since Mg^{2+} is more electropositive, the electronic cloud in each TiO_2 might be loosely held, favoring the formation of less dense anatase phase. In other words, the tight packing arrangement required for rutile phase formation is fully suppressed by the addition of magnesium nitrate in water which enhances the polarity of water, thus facilitating the formation of anatase phase exclusively. In addition, the presence of residual alkyl groups can also reduce the rate of crystallization of TiO_2 which favored the formation of less dense anatase phase.

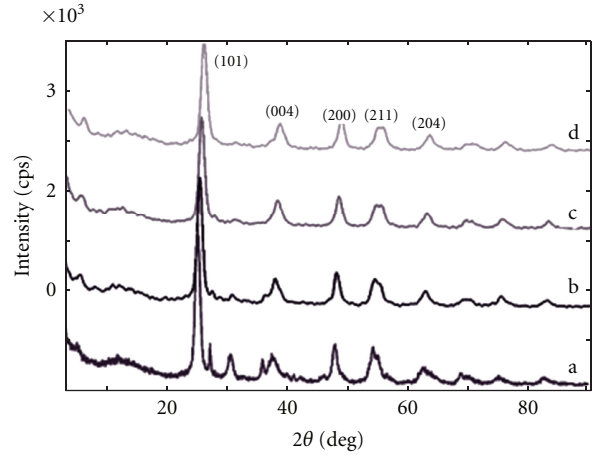

Figure 1: XRD patterns of (a) undoped TiO_2, (b) 0.75 wt.% of Mg^{2+}-doped TiO_2, (c) 1.0 wt.% of Mg^{2+}-doped TiO_2, and (d) 1.25 wt.% of Mg^{2+}-doped TiO_2.

The BET surface area results have shown that there is a much increase in surface area of doped catalysts than undoped one. With the incorporation of Mg^{2+} dopant during the sol-gel preparation technique, there was crystal growth suppression, favoring the formation of smaller TiO_2 crystallite. This effect may be attributed to the enhanced lattice strain in the doped TiO_2 network and then decrease grain growth rate.

3.2. Diffuse Reflectance Spectroscopy. The DRS of Mg^{2+}-doped TiO_2 and undoped TiO_2 samples are given in Figure 2. The spectra of undoped TiO_2 showed an absorption peak at 388 nm in the UV region. The absorption peak of the doped TiO_2 with different percentages of Mg^{2+} at 0.75 wt.%, 1.0 wt.%, 1.25 wt.%, and 1.50 wt.% shows considerable shift towards the visible region at around 400–800 nm for all the samples. The tailing absorption peaks can be considered as the extra tail states in the bandgap because Mg^{2+} was added to the TiO_2 matrix. The extension of absorption edge to longer wavelengths for Mg^{2+}/TiO_2 indicates the existence of good contact between TiO_2 and the metal (Mg^{2+}) ion grain.

The UV-Vis absorption edge and bandgap energies of the samples were determined from the reflectance [F(R)] spectra using the Kubelka-Munk (KM) formalism and the Tauc plot method [22]. The extrapolated lines for Mg^{2+}-doped TiO_2 have been given in Figure 3 and used to determine the bandgap energies for Mg^{2+}-doped TiO_2, undoped TiO_2, and Degussa P25 samples. The calculated bandgap energies are given in Table 1. The largest reduction gap is observed for catalyst containing 1.25 wt.% of Mg^{2+}-doped TiO_2. This reduction bandgap may be attributed to the doping of Mg^{2+} as impurity into the host structure (TiO_2) and create extra energy levels situated within the bandgap [23]. The extra energy level created within the bandgap due to shifting of the Fermi energy level of Mg^{2+} towards valence band since metal create P-type semiconductor.

Table 1: Crystallite size, BET surface area, and bandgap energy of each catalyst.

Catalyst no.	wt.% doping of Mg^{2+} in TiO_2	Calcination temp. (°C)	Crystallite size (nm)	BET surface area (m^2/g)	Bandgap energy (eV)
(1)	0.75	400	15.00	85.209	2.90
(2)	1.0	400	12.11	105.987	2.85
(3)	1.25	400	11.25	107.267	2.75
(4)	1.50	400	13.26	101.820	2.95
(5)	Undoped TiO_2	400	11.30	79.382	3.2
(6)	Degussa P25	—	—	69.962	3.1

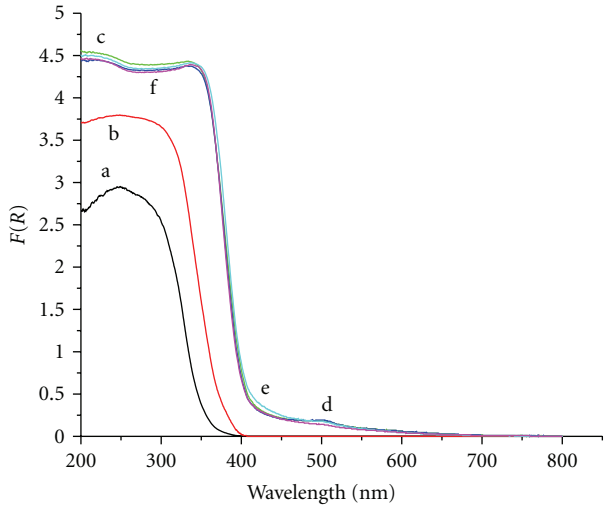

(a) Undoped TiO_2
(b) Degussa P25
(c) 0.75 wt.% of Mg^{2+}
(d) 1 wt.% of Mg^{2+}
(e) 1.25 wt.% of Mg^{2+}
(f) 1.5 wt.% of Mg^{2+}

Figure 2: The DRS-UV-Vis spectra of Degussa P25, undoped, and doped TiO_2 with different % of Mg^{2+}.

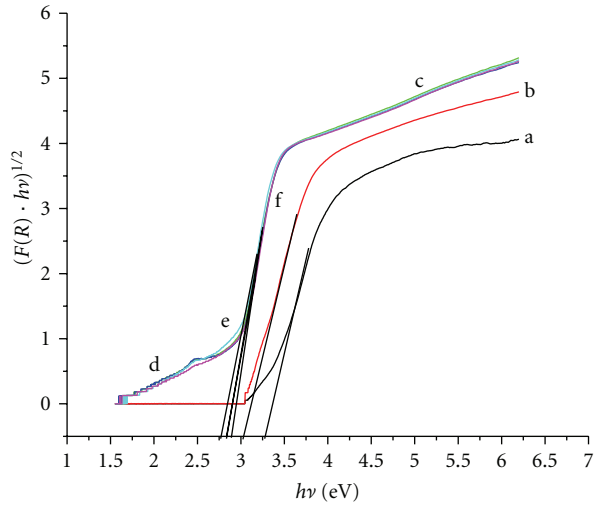

(a) Undoped TiO_2
(b) Degussa P25
(c) 0.75 wt.% of Mg^{2+}
(d) 1 wt.% of Mg^{2+}
(e) 1.25 wt.% of Mg^{2+}
(f) 1.5 wt.% of Mg^{2+}

Figure 3: Plots of transformed Kubelka-Munk functions $[F(R)\cdots \mathrm{h}\nu]^{1/2}$ versus hν for Degussa P25, undoped TiO_2, and Mg^{2+}-doped TiO_2 samples.

3.3. BET Surface Areas and Pore Distribution. The BET surface areas of the as-prepared Mg^{2+}-TiO_2 sample have been given in Table 1, and nitrogen adsorption and desorption isotherms and corresponding pore size distribution curves (inset) are given in Figure 4. It is observed that at relatively high pressures between 0.075 and 0.15 (P/P_o), the curve exhibit a hysteresis loop indicating the presence of mesopores. The shape of the hysteresis loop is of type H3, associated with particle giving rise to narrow slit shaped pores [24–27]. From Figure 4 the inset figure indicated the pore size distribution range from 20 to 35 nm. The pore volume of the as-prepared catalyst is 0.135 m^3/g. However, the existing poresarise maybe due to removal of nitrate ion and organic moiety from the metal precursors (magnesium and titanium). Due tothis, organized porous structure within the bulk sample of the catalyst may helpful in photocatalysis.

3.4. Analysis of Hydroxyl Radicals ($OH^{\bullet}$). The analysis of hydroxyl radicals has been carried out by photoluminescence technique [28]. 0.1 g of Mg^{2+}-TiO_2 in 10 ppm of coumarin solution was illuminated with visible light. The fluorescence emission spectrum excited at 428 nm from the coumarin solution was measured at every 15 min of illumination. Figure 5 shows the induction of fluorescence from 10 ppm coumarin solution. As shown in the figure, gradual increase in the fluorescence at about 500 nm for 7-hydroxycoumarin which is obtained due to reaction of OH radicals and coumarin was observed by continuous illumination of visible light on the Mg^{2+}-TiO_2 solution. The trend observed in the figure indicated that formation of the OH radicals is proportional to the irradiation time.

3.5. XPS Measurements. X-ray photoelectron spectroscopy (XPS) analysis of magnesium- (II) doped sample was performed, and high-resolution scans are shown in Figures 6(a), 6(b), and 6(c). The XPS observations show that only Mg, Ti and O elements were detected from the samples in spectrum analysis. The binding energy of Mg 2p was found

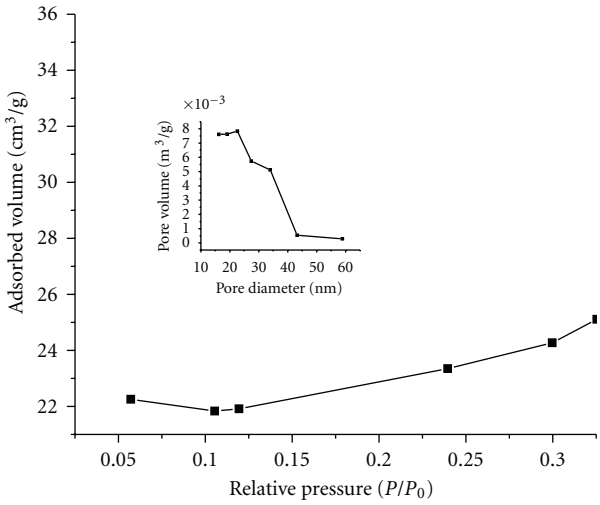

Figure 4: Nitrogen adsorption-desorption isotherms and corresponding pore size distribution. Curves (inset) of the Mg^{2+}-TiO_2 prepared at 1.25 wt.% of Mg^{2+}.

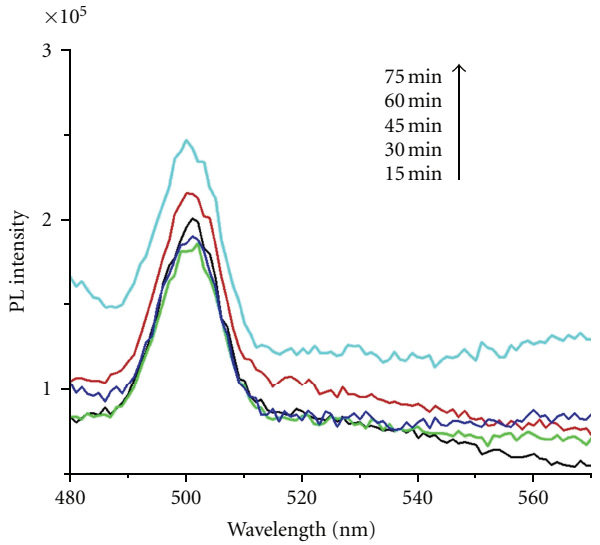

Figure 5: PL spectral changes with irradiation time on the undoped TiO_2 and 10 ppm coumarin.

to be 50.4 eV (Figure 4(a)) which is a typical of Mg^{2+} that bonded to oxygen and was assigned to the compound MgO. The binding energies of Ti $2p_{3/2}$ and Ti $2p_{1/2}$ were found to be 458.4 and 464.0 eV, and these bands could belong to Ti^{4+} (Figure 6(b)) and there was no fitting peak for Ti^{3+}. Hence the XPS-spectra confirmed the chemical composition of magnesium-doped sample to be MgO and TiO_2.

3.6. Scanning Electron Microscopy. The SEM images of TiO_2 and metal-doped TiO_2 catalysts are shown in Figures 7(a) and 7(b). The image of samples containing 1.25 wt.% of Mg^{2+} ion shows the morphological changes induced by the addition of alkaline earth cation. The catalysts are found to

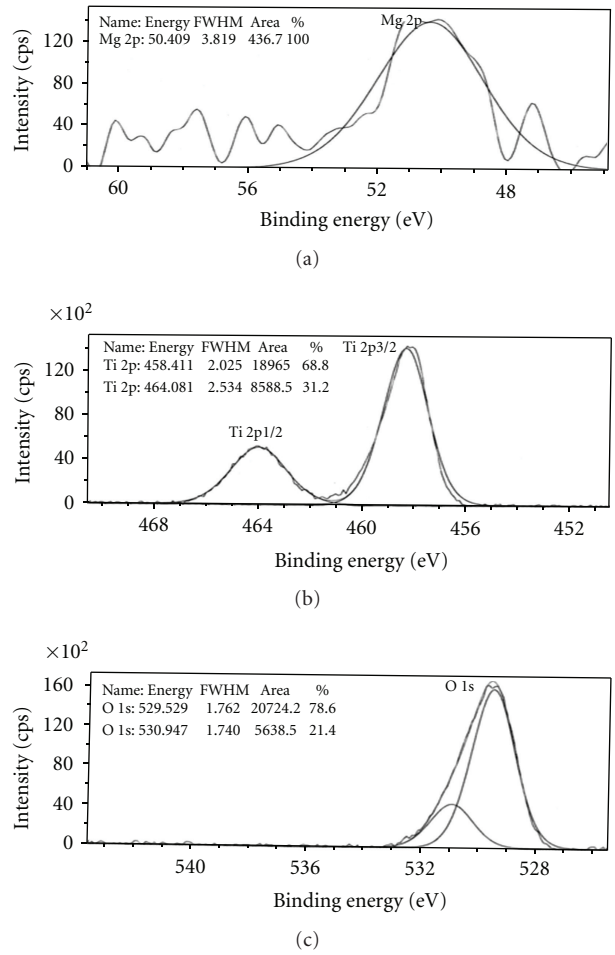

Figure 6: (a) High resolution of Mg 2p spectrum, (b) high resolution of Ti 2p spectrum, and (c) high resolution of O 1s spectrum.

contain irregular-shaped particles which are again aggregates of tiny crystals. Figure 7(a) shows anatase (undoped TiO_2) produced with no addition of magnesium ion. The sample appears as large blocks of coarse material of dimensions from around 1 to 20 μm. Figure 7(b) shows sample containing 1.25 wt.% of Mg^{2+}, with reduction in the particle size to 1–10 μm range. This clearly illustrates the altered morphology of the catalyst powders, which consists of a large portion of submicron-sized particles.

3.7. FT-IR Spectral Study. FT-IR spectra of undoped TiO_2 and 1.25 wt.% of Mg^{2+}-TiO_2 given in Figures 8(a) and 8(b) have shown peaks corresponding to stretching vibrations of O–H and bending vibrations of adsorbed water molecules around 2322–3317 cm^{-1} and 1613 cm^{-1}, respectively. The intensity of the peaks became less in Mg^{2+}-TiO_2, indicating the removal of large portion of adsorbed water from TiO_2.

The broad band below 456.06 cm^{-1} of undoped TiO_2 is due to Ti–O–Ti vibration. This peak has been shifted to 470.63 cm^{-1} in Mg-doped TiO_2 which may be because of Ti–O–Mg vibration. Hence the FT-IR spectral study along with XPS established the substitution of Mg^{2+} into TiO_2 lattice.

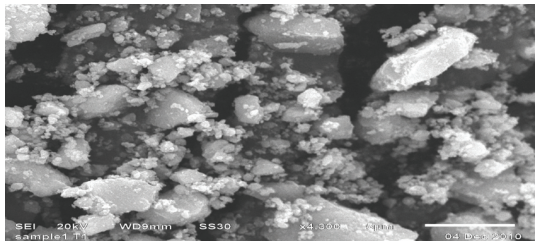

(a)

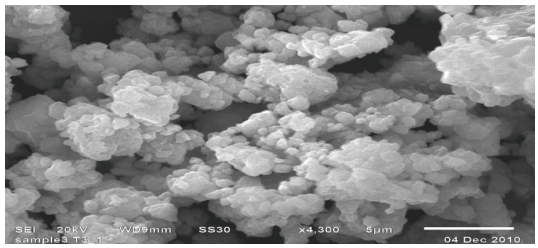

(b)

Figure 7: SEM images of (a) undoped TiO_2 and (b) 1.25 wt.% of Mg-doped TiO_2.

3.8. Photocatalytic Degradation of Dichlorvos. To understand the photocatalytic activity of the prepared catalysts, degradation of dichlorvos pesticide under the irradiation of visible light has been carried out, in the presence and absence of catalysts. The percentage of DDVP degradation is significantly less in the absence of catalyst (0.05% for 9 hours irradiation) when compared to that of undoped or doped titanium dioxide. A blank experiment in the absence of irradiation along with catalysts demonstrated that no significant change in the DDVP concentration was observed. The efficiency of photocatalytic degradation process depends on various experimental parameters such as effect of dopant concentration, pH, catalyst dosage, and initial concentration of pollutant. Hence, it is essential to optimize these parameters to achieve higher degradation efficiency of photocatalyst.

3.8.1. Effect of Mg Dopant Concentration on Photocatalytic Degradation of DDVP. Figure 9 shows the results of the photocatalytic degradation of DDVP by irradiation of visible light over Degussa P25, undoped TiO_2 catalyst, and Mg-doped TiO_2 photocatalyst with different doping concentrations of Mg in TiO_2. Among various concentrations of Mg, 1.25 wt.% of Mg-TiO_2 catalyst exhibits the highest photocatalytic activity. This may be attributed to that increase in dopant concentration leads to increase in number of trapped charge carriers per particle [15, 29] and is the highest in 1.25 wt.% of Mg^{2+}-TiO_2 which is the optimum concentration showing maximum photocatalytic activity.

The results of the experiment show that the rate of phosphate ion formation increased with increase in the concentration of magnesium ions, and it was optimum at 1.25 wt.%. However, magnesium ions' doping became detrimental when the dopant concentration was above 1.25 wt.%.

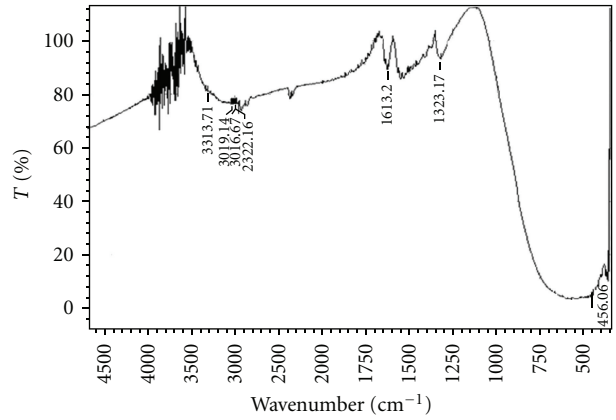

(a)

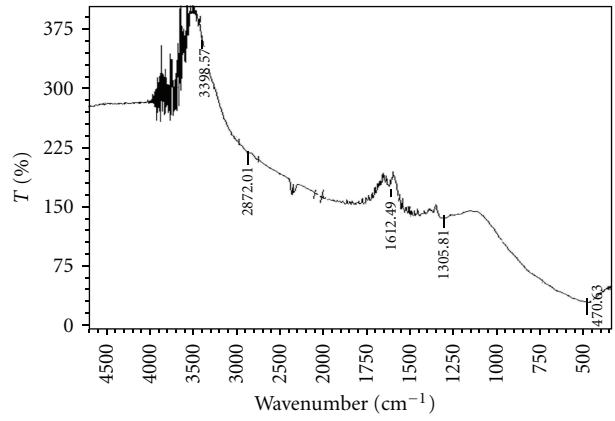

(b)

Figure 8: FT-IR spectra of (a) undoped TiO_2 and (b) 1.25 wt.% Mg^{+2}-TiO_2.

It also demonstrates that, even though the concentration of the doped magnesium ions is small, it still gives much influence on the photocatalytic activity of TiO_2 particles.

3.8.2. Effect of pH. The adsorption properties of catalysts can be greatly changed at different pH values; hence, the catalyst-assisted photodegradation of DDVP has also been monitored by in situ measurements of pH of the aqueous solution with irradiation time, at a fixed weight of catalyst and DDVP pesticide concentration at different pH values. Solution pH influences adsorption and desorption of the substrate, catalyst surface charge, oxidation potential of the valence band, and other physicochemical properties.

The effect of pH on the photocatalytic degradation of DDVP is shown in Figure 10. The degradation plot for DDVP has been plotted between rate constant and pH of the solution. Based on the results, it is observed that the rate of degradation decreased with increase in pH of the solution. The optimum pH of the solution for the degradation of DDVP is 2. Generally in acidic pH the surface of the TiO_2 is in the form of $TiOH_2^+$. The photogenerated electrons can be captured by the adsorbed H^+ to form $H^{\bullet}_{ads}$. At higher pH,

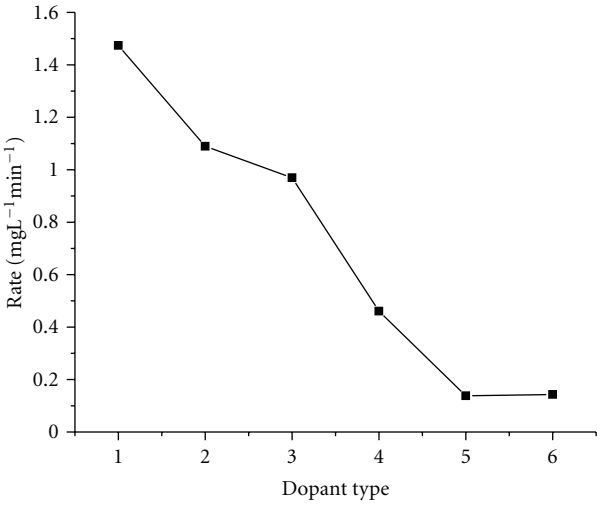

Figure 9: Effect of dopant concentration on the degradation of dichlorvos. Catalyst dosage = 0.10 g, pH = 3, and [DDVP] = 150 ppm.

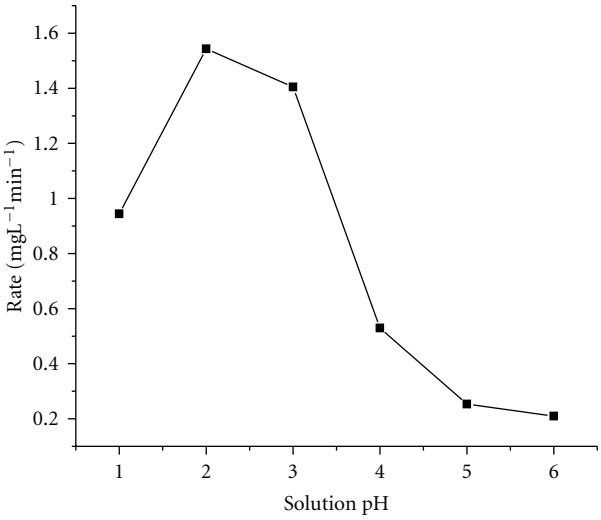

Figure 10: The effect of pH on the degradation of dichlorvos by Mg^{2+}-doped TiO_2. Catalyst dosage = 0.10 g, [DDVP] = 150 ppm.

the surface of catalyst has a net negative charge as TiO_2^-, and hence the degradation rate was found to be lower:

$$\begin{aligned} \mathrm{TiOH} + \mathrm{H^+} &\longrightarrow \mathrm{TiOH_2^+}, \quad \mathrm{pH} < 6.25, \\ \mathrm{TiOH} &\longrightarrow \mathrm{TiO^-} + \mathrm{H^+}, \quad \mathrm{pH} > 6.25. \end{aligned} \tag{3}$$

3.8.3. Effect of Catalyst Dosage. The effect of the amount of catalyst on the photodegradation rate was investigated at a fixed pH and initial concentration of the dichlorvos, experiments were performed with varying amounts of Mg^{2+}-TiO_2 from 0.025 g to 0.3 g in 100 mL DDVP pesticide aqueous solution. The degradation pattern from such experiments has been depicted in Figure 11, which reveals that the rate of degradation increases linearly with increase in the amount of catalyst up to 0.1 g and then decreases. This may be explained by two main reasons. The first one is due to the presence of foreign metal ions (Mg^{2+}) as dopant that helps in inhibiting electron-hole pair recombination and enhancing interfacial charge transfer reactions, which leads to increased catalytic activity.

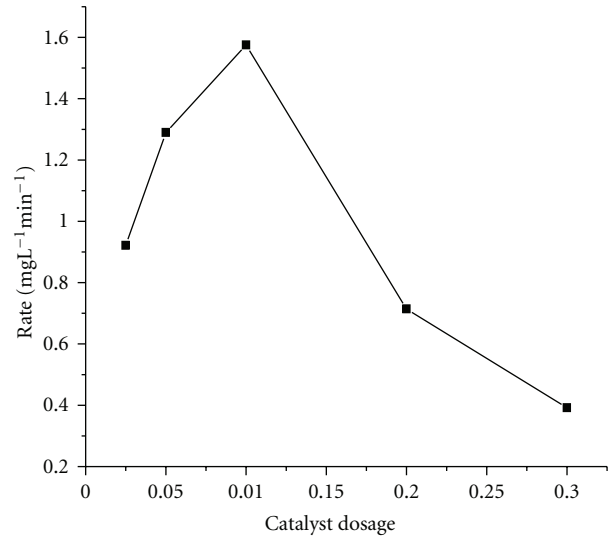

Figure 11: The effect of catalyst dosage on the degradation of dichlorvos by Mg^{2+}-doped TiO_2, pH = 2, [DDVP] = 150 ppm.

Secondly, as the amount of catalyst increases, the number of photons absorbed and the number of DDVP molecules adsorbed are increased leading to the increase in DDVP degradation. At higher concentrations of catalyst, although more surface areas are available for constant DDVP molecules, the solution turbidity increases and it interferes with the penetration of light. The deactivation of activated molecules by collision with ground-state molecules may also hinder the photocatalytic efficiency [30]. Hence, above a certain level, additional catalyst amount is not involved in catalysis, and thus the rate levels off.

3.8.4. Effect of Initial Pesticide Concentration. At a fixed weight of Mg^{2+}-TiO_2 and pH, variation of initial pesticide concentration on photo degradation was studied and shown in Figure 12. It was noted that the degradation rate increases with the increase of pesticide concentration up to a certain concentration (150 ppm), and a further increase leads to a decrease in the pesticide degradation rate. This is due to the reduction of generation of radicals ($OH^\bullet$) on the catalyst surface since the active surfaces are covered by pesticide molecules.

3.9. Photocatalytic Mechanism. Based on the experimental results and reports of the previous workers, the following

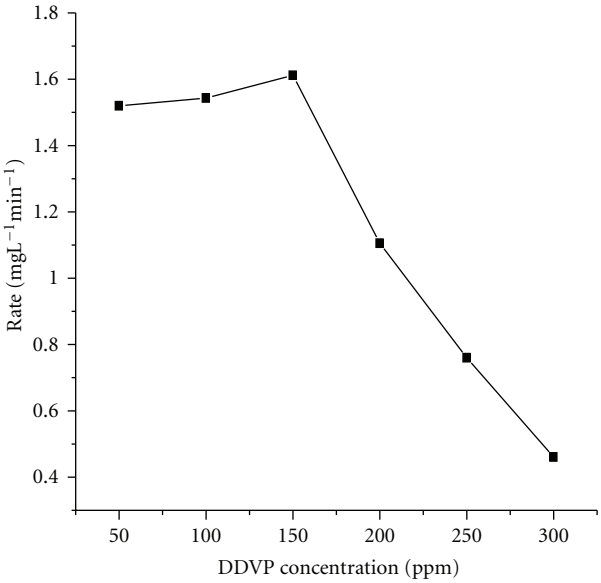

Figure 12: The effect of concentration of DDVP on the degradation of dichlorvos by Mg^{2+}-doped TiO_2, pH = 2, catalyst dosage = 0.10 g.

mechanism would be proposed for the photocatalytic reactions of magnesium-doped TiO_2 [31–33].

(a) Upon visible light illumination of photocatalyst, electrons are ejected from the valence band to the conduction band leaving positive holes in the valence band.

(b) When the metal ion doped into TiO_2 lattice, it trapped the ejected electrons, holding up the recombination process.

(c) The trapped electrons can be further scavenged by molecular oxygen, which is adsorbed on the TiO_2 surface to generate superoxide radical, and this in turn produces hydrogen peroxide (H_2O_2), hydroperoxy ($HO_2^{\bullet}$), and hydroxyl ($^{\bullet}OH$) radicals.

(d) The positive holes in the valence band act as good oxidizing agents available for degradation of pesticide in the solution. Thus, the DDVP is attacked by the hydroxyl radicals formed both by trapped electrons and hole in the VB as given in the above equations, to generate phosphate ions, organic radicals, or other intermediates, which further undergo degradation.

4. Conclusions

The DRS analysis shows that doping of Mg^{2+} into TiO_2 shifts the absorbance band of TiO_2 from UV to visible region, and the bandgap energy is reduced for all doped catalysts (from 3.2 eV to 2.75 eV); the largest reduction gap was observed for doped catalyst of 1.25 wt.% of Mg. The incorporation of Mg^{2+} ions into the TiO_2 was evidenced by XPS analysis. The BET results also show that there is an increase in surface area of the catalyst, which enhances the photocatalytic degradation of DDVP in visible light. The present work imparts the significance of magnesium ion doping into titania, in dichlorvos degradation. It also establishes the doping of magnesium by sol-gel as a best alternative method. The experimental results show that the photocatalytic activity of undoped TiO_2 is lower than magnesium-doped TiO_2.

Magnesium doping causes better separation of electron and holes on the modified TiO_2 surface allowing more efficient channeling of the produced electrons into useful redox reactions, thus enhancing the DDVP degradation in the presence of visible light, when compared to undoped TiO_2 which can be excited only in less available UV light. The degradation of DDVP was maximum at 150 ppm DDVP concentration, 0.1 g of Mg^{2+}-TiO_2 catalyst, and at a pH of 2 using 1.25 wt.% of magnesium-doped titania catalyst.

Acknowledgments

T. Rao and Mrs. T. Susmitha are thankful to UGC, New Delhi, for financial assistance as major research project to carry out research work and also thankful to Dr. Sridhar, Scientist, IICT, Hyderabad, for providing XPS spectral data. T. A. Segne is also thankful to the Ethiopian Government for their financial support for doing Ph.D. at the Andhra University, Visakhapatnam, India.

References

[1] O. Legrini, E. Oliveros, and A. M. Braun, "Photochemical processes for water treatment," *Chemical Reviews*, vol. 93, no. 2, pp. 671–698, 1993.

[2] D. Chen and A. K. Ray, "Photocatalytic kinetics of phenol and its derivatives over UV irradiated TiO_2 ," *Applied Catalysis B*, vol. 23, no. 2-3, pp. 143–157, 1999.

[3] A. L. Linsebigler, G. Lu, and J. T. Yates, "Photocatalysis on TiO_2 surfaces: principles, mechanisms, and selected results," *Chemical Reviews*, vol. 95, no. 3, pp. 735–758, 1995.

[4] C. Minero, E. Pelizetti, P. Pichat, M. Sega, and M. Vincenti, "Formation of condensation products in advanced oxidation technologies: the photocatalytic degradation of dichlorophenols on TiO_2 ," *Environmental Science and Technology*, vol. 29, no. 9, pp. 2226–2234, 1995.

[5] P. K. J. Robertson, "Semiconductor photocatalysis: an environmentally acceptable alternative production technique and effluent treatment process," *Journal of Cleaner Production*, vol. 4, no. 3, pp. 203–212, 1996.

[6] A. Fujishima and K. Honda, "Electrochemical photolysis of water at a semiconductor electrode," *Nature*, vol. 238, no. 5358, pp. 37–38, 1972.

[7] R. W. Matthews, "Photooxidation of organic impurities in water using thin films of titanium dioxide," *Journal of Physical Chemistry*, vol. 91, no. 12, pp. 3328–3333, 1987.

[8] M. A. Fox, C. C. Chen, K. Park, and J. N. Younathan, "Controlled organic redox reactivity on irradiated semiconductor surfaces," *ACS Symposium Series*, vol. 278, pp. 69–78, 1985.

[9] A. Mills, R. H. Davies, and D. Worsley, "Water purification by semiconductor photocatalysis," *Chemical Society Reviews*, vol. 22, no. 6, pp. 417–425, 1993.

[10] S. Peng, Y. Li, F. Jiang, G. Lu, and S. Li, "Effect of Be^{2+} doping TiO_2 on its photocatalytic activity," *Chemical Physics Letters*, vol. 398, no. 1–3, pp. 235–239, 2004.

[11] M. R. Hoffmann, S. T. Martin, W. Choi, and D. W. Bahnemann, "Environmental applications of semiconductor photocatalysis," *Chemical Reviews*, vol. 95, no. 1, pp. 69–96, 1995.

[12] Y. Ku, W. Wang, and Y. S. Shen, "Reaction behaviors of decomposition of monocrotophos in aqueous solution by UV and UV/O_3 processes," *Journal of Hazardous Materials*, vol. 72, no. 1, pp. 25–37, 2000.

[13] C. Kormann, D. W. Bahnemann, and M. R. Hoffmann, "Preparation and characterization of quantum-size titanium dioxide," *Journal of Physical Chemistry*, vol. 92, no. 18, pp. 5196–5201, 1988.

[14] J. Moser and M. Grätzel, "Photosensitized electron injection in colloidal semiconductors," *Journal of the American Chemical Society*, vol. 106, no. 22, pp. 6557–6564, 1984.

[15] W. Choi, A. Termin, and M. R. Hoffmann, "The role of metal ion dopants in quantum-sized TiO_2: correlation between photoreactivity and charge carrier recombination dynamics," *Journal of Physical Chemistry*, vol. 98, no. 51, pp. 13669–13679, 1994.

[16] Q. Xiang, J. Yu, and M. Jaroniec, "Graphene based semiconductor photocatalysis," *Chemical Society Reviews*, vol. 41, no. 2, pp. 782–796, 2012.

[17] Y. Bessekhouad, D. Robert, J. V. Weber, and N. Chaoui, "Effect of alkaline-doped TiO_2 on photocatalytic efficiency," *Journal of Photochemistry and Photobiology A*, vol. 167, no. 1, pp. 49–57, 2004.

[18] S. Liu, J. Yu, and M. Jaroniec, "Anatase TiO_2 with dominant high-energy {001} facets: synthesis, properties and applications," *Chemistry of Materials*, vol. 23, no. 18, pp. 4085–4093, 2011.

[19] E. D. Booth, E. Jones, and B. M. Elliott, "Review of the in vitro and in vivo genotoxicity of dichlorvos," *Regulatory Toxicology and Pharmacology*, vol. 49, no. 3, pp. 316–326, 2007.

[20] E. Evgenidou, K. Fytianos, and I. Poulios, "Semiconductor-sensitized photodegradation of dichlorvos in water using TiO_2 and ZnO as catalysts," *Applied Catalysis B*, vol. 59, no. 1-2, pp. 81–89, 2005.

[21] T. Wu, G. Liu, J. Zhao, H. Hidaka, and N. Serpone, "TiO_2 assisted degradation of dyes IX: photooxidation of asquarylium cyanine dye in aqueous dispersions under visible light irradiation," *Environmental Science and Technology*, vol. 33, no. 9, pp. 1379–1387, 1999.

[22] D. Blake, "Bibliography of work on the heterogeneous photocataloytic removal of hazardous compounds from water and air," Tech. Rep. NREL/TP-510-31319, National Technical Information Service, United States, Department of Commerce, 2001.

[23] W. Wang, J. Zhang, F. Chen, D. He, and M. Anpo, "Preparation and photocatalytic properties of Fe^{3+} Ag@TiO_2 core-shell nanoparticles," *Journal of Colloid and Interface Science*, vol. 323, no. 1, pp. 182–186, 2008.

[24] K. S. W. Sing, D. H. Everett, R. A. W. Haul et al., "Reporting physisorption data for gas/solid interface with special reference to the determination of surface area and porosity," *Pure and Applied Chemistry*, vol. 57, pp. 603–319, 1985.

[25] S. J. Gregg and K. S. W. Sing, *Adsorption, Surface Area and Poracity*, Academic Press, New York, NY, USA, 1982.

[26] J. Yu, J. C. Yu, K.-P. Mitch et al., "Effects of acidic and basic hydrolysis catalysts on the photocatlytic activity and structures of bimodal mesoporous titania," *Journal of Catalysis*, vol. 217, no. 1, pp. 69–78, 2003.

[27] J. Yu, S. Liu, and H. Yu, "Microstructures and photoactivity of mesoporous anatase hollow microspheres fabricated by fluoride-mediated self-transformation," *Journal of Catalysis*, vol. 249, no. 1, pp. 59–66, 2007.

[28] Q. Xiang, J. Yu, and P. K. Wong, "Quantitative characterization of hydroxyl radicals produced by various photocatalysts," *Journal of Colloid and Interface Science*, vol. 357, no. 1, pp. 163–167, 2011.

[29] B. Neppolian, H. C. Choi, S. Sakthivel, B. Arabindoo, and V. Murugesan, "Solar/UV-induced photocatalytic degradation of three commercial textile dyes," *Journal of Hazardous Materials*, vol. 89, no. 2-3, pp. 303–317, 2002.

[30] J. M. Herrmann and C. Guillard, "Photocatalytic degradation of pesticides in agricultural used waters," *Comptes Rendus de l'Académie des Sciences IIC*, vol. 3, no. 6, pp. 417–422, 2000.

[31] H. Li, X. Duan, G. Liu, and L. Li, "Synthesis and characterization of copper ions surface-doped titanium dioxide nanotubes," *Materials Research Bulletin*, vol. 43, no. 8-9, pp. 1971–1981, 2008.

[32] K. Chiang, R. Amal, and T. Tran, "Photocatalytic degradation of cyanide using titanium dioxide modified with copper oxide," *Advances in Environmental Research*, vol. 6, no. 4, pp. 471–485, 2002.

[33] Y. Yang, Q. Wu, Y. Guo, C. Hu, and E. Wang, "Efficient degradation of dye pollutants on nanoporous polyoxotungstate-anatase composite under visible-light irradiation," *Journal of Molecular Catalysis A*, vol. 225, no. 2, pp. 203–212, 2005.

Hindawi Publishing Corporation
Advances in Materials Science and Engineering
Volume 2012, Article ID 510123, 5 pages
doi:10.1155/2012/510123

Research Article

Optimization of Nano-TiO_2 Photocatalytic Reactor for Organophosphorus Degradation

Ilin Sadeghi,[1] Pooya Arbab,[2] Mahdi Fathizadeh,[1] Hoseen Fakhraee,[2] and Mahdi Amrollahi[3]

[1] *Department of Chemical Engineering, Amirkabir University of Technology (Tehran Polytechnic), Hafez Ave., P.O. Box 15875-4413, Tehran, Iran*
[2] *Department of Civil Engineering, University of Science and Technology, Tehran, Iran*
[3] *Department of Polymer Engineering, Islamic Azad University, Omidiyeh Branch, Khuzestan, Iran*

Correspondence should be addressed to Mahdi Fathizadeh, m.fathizade@aut.ac.ir

Received 5 January 2012; Revised 14 February 2012; Accepted 20 February 2012

Academic Editor: Guohua Jiang

The photocatalytic decontamination of triethyl phosphate (TEP) is studied by the UV/nano-TiO_2 process. The nano-TiO_2 concentration and pH value for the complete oxidation of TEP were investigated in different concentrations of TEP. The kinetic reaction was calculated for TEP as a function of initial concentration of TEP. Results of adsorptions showed that TEP was adsorbed better in alkalinity pH, and the natural pH had the highest reaction rate for complete degradation. Also, the zero-kinetic order with the lag time as a function of initial concentration of TEP and TiO_2 was suggested for oxidation of TEP. The optimized concentration of nano-TiO_2 was 400 mg/lit which had the best conversion and the lowest lag time in the reaction.

1. Introduction

Nowadays, an important environmental constrain is the effort to improve water quality and remove pollution from waste water. One of the most widespread methods of water purification is biodegradation which has a low reaction rate [1–3]. A novel method that has become popular in recent decades is the advanced oxidation processes (AOPs) which are very potent in oxidization, decolorization, mineralization, reducing heavy metals, and degrading organic pollutants [2–4].

Organophosphate is a very complicated contaminant in waste water which contains insecticides, pesticides, and detergents. These types of pollutants are found in industrial, agricultural, and also domestic waste water. Organophosphate degrades to several intermediate materials; phosphate appears as a solution when it degrades completely. The triethyl phosphate (TEP) is an organophosphate used as an industrial catalyst, a polymer resin modifier, a plasticizer, an intermediate for pesticides and other chemicals, a stabilizer for peroxides, a strengthening agent for rubbers and plastics including vinyl polymers and unsaturated polyesters, and so forth [4–8]. The intermediate products of TEP degradation are diethyl phosphate and monoethyl phosphate which are known as pollutants in wastewater. The final products of TEP degradation are phosphate, carbon dioxide, and water. Therefore, it can be said that phosphate can see end of TEP degradation [9].

One of the most common AOPs methods for both academic and industrial researches is photocatalytic process [10, 11]. TiO_2 photocatalyst was considered as one of the most practical candidates due to its high stability and photocatalytic efficiency [12–14]. Recently, more attention has been paid to increasing the reaction rate and enhance its catalytic efficiency [15–17]. Several reports have been presented for the nano-TiO_2 photocatalytic process; the effects of important parameters such as pH values, TiO_2 dosage, light intensities, dissolved oxygen levels and other operating conditions were investigated for heavy metals and some organic materials [17–21]. There is not any report on optimization of effective parameters for degradation of organophosphates which are important factors for photocatalytic reactor design; therefore, a study on the optimization of effective parameters is important and promising, which is yet to be done.

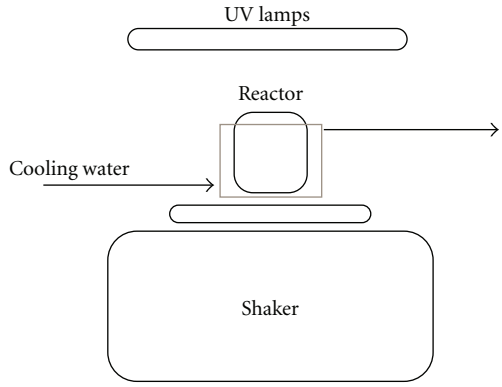

Figure 1: Schematic diagram of the photocatalytic system.

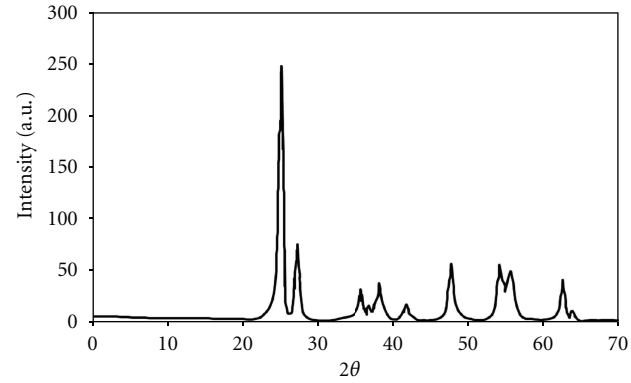

Figure 2: The XRD pattern of nano-TiO_2 particle.

In this research, the decontamination of organophosphates by the UV/nano-TiO_2 process has been investigated, and optimized conditions have been obtained. Firstly, nano-TiO_2 particles were characterized by X-ray powder diffraction (XRD), Field-Emission Scanning Electron Microscope (FESEM), and Dynamic Light Scattering (DLS), and the best pH for TEP adsorption was calculated in dark condition. Then, the optimum concentration of nano-TiO_2 and pH in photocatalytic process was studied. At the end, the kinetic reaction of TEP degradation was suggested as a function of initial concentration of TEP, nano-TiO_2 concentration and pH.

2. Experimental

2.1. Materials. Triethyl phosphate (TEP) with purity above 99.5%, sodium hydroxide (NaOH) and nitric acid were obtained from Merck Co. (Germany). Titanium dioxide nanoparticle (P-25, ca. 80% anatase and 20% rutile) with an average particle size of 20 nm and a BET surface area of 50.4 m^2g^{-1} was supplied by Degussa, Germany.

2.2. Analysis. The phosphate concentration was measured by a UV/visible spectrophotometer at a wavelength of 640 nm. The samples were filtered to remove nanoparticles of nano-TiO_2 particles. The gas chromatograph (GC) was equipped with a flame-ionization detector and a WCOT fused silica column (50 m × 250 μm × 0.4 μm) to measure the TEP concentration.

The X-ray diffraction (XRD) pattern was obtained using a Philips X'Pert diffractometer (X'pert diffractometer using CuK α radiation). The average crystal dimension was calculated using Scherrer's equation, which was also confirmed with DLS test. The FESEM (Hitachi, model S-4160) was used to determine the particle size distribution of nano-TiO_2 crystals.

2.3. Adsorption Measurements. The oxidation of TEP was carried out in a glass batch reactor with six 15 W UV-C lamps at 25.0 ± 0.1°C (Figure 1). The concentration of nano-TiO_2 and TEP was changed from 100 to 1000 mg L^{-1} and from 10 to 50 mg L^{-1}, respectively. The adsorption value measurements were carried out with 400 mg/L nano-TiO_2 in dark condition. The pH of solution was stabled with 0.1 M of NaOH and HNO_3 solutions. For complete degradation of TEP, the phosphate concentration was measured during the reaction.

Table 1: Adsorption of TEP on nano-TiO_2 surface (nano-TiO_2 = 0.4 g L^{-1}, TEP = 30 mg L^{-1}).

pH value	2	4	7	10	12
TEP	14.01 ± 0.5	22.3 ± 0.7	24.7 ± 0.7	27.2 ± 0.7	34.02 ± 0.7

3. Results and Discussion

3.1. Structure and Surface Characterization of TiO_2. The XRD patterns of the nano-TiO_2 in rutile and anatase phases are shown in Figure 2. The XRD patterns exhibit strong diffraction peaks at 27°, 36°, and 55°. Ordinary peaks seen at 25° and 48° indicate that TiO_2 has been in the rutile and the anatase phase with the ratio of approximately 20 : 80, respectively. Also, the Degussa materials were random spherical nanomaterials 10–50 nm in size and composed of a mixture of ~8 : 2 anatase (JCPDS card no. 00-21-1272): rutile (JCPDS card no. 00-21-1276). The crystallite size of the prepared particles obtained from the width of XRD peaks using Scherrer's equation is 20 nm, which can be confirmed with DLS FESEM image (Figure 3).

3.2. Adsorption of TEP and Cr(VI) Mixture on TiO_2. The effect of the pH values on adsorption behaviour of TEP on nano-TiO_2 particles was investigated. TEP adsorptions percentages at different pH levels are shown in Table 1. At the pH value of 12, the adsorption of TEP on nano-TiO_2 particles is the highest and minimum percentage of TEP adsorption is seen at the pH value of 2. In the acidic pH, TEP is protonized to carry the positive charges, while the surface of TiO_2 is electropositive [8]. Therefore, the acidic pH does not favour the adsorption of TEP on the TiO_2 particles.

3.3. Photocatalytic Degradation of TEP by UV/TiO_2. The intermediate materials such as diethyl phosphate and ethanol

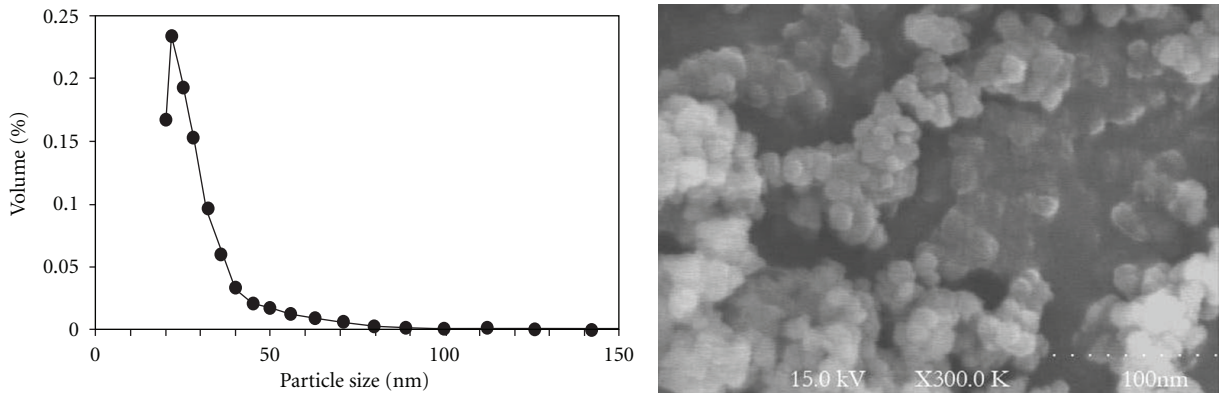

(a) (b)

Figure 3: FESEM image and particle size distribution of nano-TiO_2 patricle.

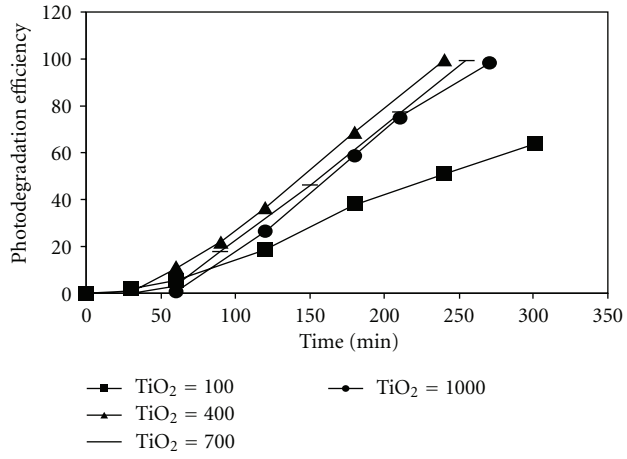

Figure 4: Effect of nano-TiO_2 concentration on TEP degredation (TEP = 30 mg/li, pH = 7).

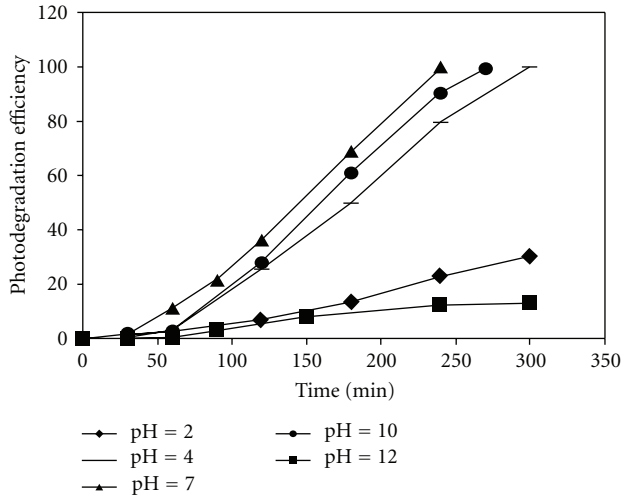

Figure 5: The effect of pH on reaction rate (TEP = 30 mg/li and nano-TiO_2 = 400 mg/li).

are produced from TEP photocatalytic degradation, and subsequently monoethyl phosphate is formed from TEP and diethyl phosphate. In the final step, TEP and intermediate products degrade to phosphate, which is known as the end of TEP degradation. To study the photocatalytic reduction of TEP by UV/TiO_2 process, the kinetic experiments were carried out at different pH values, TEP and nano-TiO_2 concentration by analyzing the phosphate concentration. The effect of nano-TiO_2 concentration on photocatalytic reaction is shown in Figure 4. In the high concentration of nano-TiO_2 (1000 mg/li), the solution is very dark, which decreases diffusion zone of UV radiation in the solution and causes the reaction rate to decline. On the other hand, low concentration of nano-TiO_2 causes the reaction zone to decrease. Therefore, the best concentration of nano-TiO_2 is 400 mg/lit which shows the highest reaction rate.

The effect of pH values on reaction rates is shown in Figure 5. At acidic pH values, because of proton releasing in solution, the photocatalytic reaction rate is higher than alkaline pH. Therefore, it hardly reaches the criteria for ready photocatalytic degradation. Also, the adsorption of TEP over the nano-TiO_2 particles is another crucial factor in the photocatalytic reaction rate. Increasing the amount of TEP adsorption leads to more TEP concentration in the reaction zone which can improve the reaction rate. The experimental results show that natural pH has the highest reaction rate. Degradation rate of TEP at lower pH values is lower than that of at pH value of 7.0. This can be explained by the less adsorption amount of TEP on the TiO_2 at acidic pH compared to the pH value of 7; therefore, it can be said that the adsorption process plays an important role in photocatalytic reactions.

In Figure 6, the effect of TEP concentration on kinetic degradation is shown at the pH level of 7. A little trace of phosphate is observed at an early stage of the photocatalytic reaction because phosphate forms after the degradation of TEP, diethyl phosphate, and monoethyl phosphate. After a lag time, phosphate amount suddenly increases up to final concentration. These lags were 21.1, 35, and 47 min

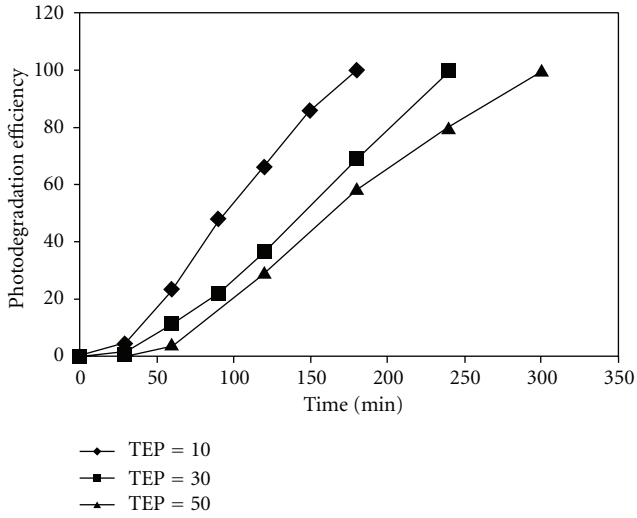

FIGURE 6: The kenetic rate of TEP (nano-TiO_2 = 400 mg/li and pH = 7).

for 10, 30, and 50 mg L^{-1} of TEP concentration in solution, respectively.

The effects of TiO_2 and TEP concentration were studied, and the results are shown in Figure 6. The photocatalytic reaction rate is very low in low concentration of nano-TiO_2 (100 mg/li). As the concentration of nano-TiO_2 increases to 400 mg/li, the reaction rate rise to the highest value. Results show that the reaction rate is only as a function of initial TEP concentration and TiO_2 does not have any effect on it. Also, it can be seen that total degradation of TEP has a lag time which is as a function initial concentration of TEP and TiO_2 concentration. The suggested kinetic reaction is a zero-order equation with a lag time as a function of initial concentration of TEP. The final equation is

$$\frac{dC_{\text{phosphate}}}{dt} = k_{\text{red}}, \quad t > t_{\text{lag}}, \tag{1}$$

where $k_{\text{red}} = 0.756C_{\text{TEP}_0}^{-0.29}$ (hr^{-1}) and $t_{\text{lag}} = 0.567C_{\text{TiO}_2}^{0.454}C_{\text{TEP}_0}^{0.492}$ (hr).

4. Conclusion

The optimum condition of TEP degradation in nano-TiO_2 photocatalytic reaction was obtained. Also, effects of nano-TiO_2 and TEP concentration as well as pH values were studied using a batch reactor. The results show that the neutral pH has highest photocatalytic reaction rate while the highest TEP adsorption is calculated at alkaline pH. Also, increasing the concentration of nano-TiO_2 declines the photocatalytic reaction rate and rises the lag time which was seen as TEP concentration increased. At the end, a zero-order kinetic reaction rate with a lag time was suggested for complete oxidation of TEP.

Acknowledgments

The authors are thankful for the financial support of the Department of Chemical Engineering, Amirkabir University of Technology (Tehran Polytechnic), Tehran, Iran, and Mr. Pooya Arbab for their cooperation.

References

[1] R. Thiruvenkatachari, S. Vigneswaran, and I. S. Moon, "A review on UV/TiO_2 photocatalytic oxidation process," *Korean Journal of Chemical Engineering*, vol. 25, no. 1, pp. 64–72, 2008.

[2] T. van Gerven, G. Mul, J. Moulijn, and A. Stankiewicz, "A review of intensification of photocatalytic processes," *Chemical Engineering and Processing*, vol. 46, no. 9, pp. 781–789, 2007.

[3] R. Andreozzi, V. Caprio, A. Insola, and R. Marotta, "Advanced oxidation processes (AOP) for water purification and recovery," *Catalysis Today*, vol. 53, no. 1, pp. 51–59, 1999.

[4] S. Bang, M. Patel, L. Lippincott, and X. Meng, "Removal of arsenic from groundwater by granular titanium dioxide adsorbent," *Chemosphere*, vol. 60, no. 3, pp. 389–397, 2005.

[5] R. A. Wuana, F. E. Okieimen, and J. A. Imborvungu, "Removal of heavy metals from a contaminated soil using chelating organic acids," *International Journal of Environmental Science and Technology*, vol. 7, no. 3, pp. 485–496, 2010.

[6] S. Malato, J. Blanco, A. R. Fernández-Alba, and A. Agüera, "Solar photocatalytic mineralization of commercial pesticides: acrinathrin," *Chemosphere*, vol. 40, no. 4, pp. 403–409, 2000.

[7] J. P. Percherancier, R. Chapelon, and B. Pouyet, "Semiconductor-sensitized photodegradation of pesticides in water: the case of carbetamide," *Journal of Photochemistry and Photobiology A*, vol. 87, no. 3, pp. 261–266, 1995.

[8] X. R. Xu, H. B. Li, and J. D. Gu, "Simultaneous decontamination of hexavalent chromium and methyl tert-butyl ether by UV/TiO_2 process," *Chemosphere*, vol. 63, no. 2, pp. 254–260, 2006.

[9] E. A. Kozlova, P. G. Smirniotis, and A. V. Vorontsov, "Comparative study on photocatalytic oxidation of four organophosphorus simulants of chemical warfare agents in aqueous suspension of titanium dioxide," *Journal of Photochemistry and Photobiology A*, vol. 162, no. 2-3, pp. 503–511, 2004.

[10] X. Wang, S. O. Pehkonen, and A. K. Ray, "Removal of aqueous Cr(VI) by a combination of photocatalytic reduction and coprecipitation," *Industrial and Engineering Chemistry Research*, vol. 43, no. 7, pp. 1665–1672, 2004.

[11] F. Jiang, Z. Zheng, Z. Xu, S. Zheng, Z. Guo, and L. Chen, "Aqueous Cr(VI) photo-reduction catalyzed by TiO_2 and sulfated TiO_2 ," *Journal of Hazardous Materials*, vol. 134, no. 1–3, pp. 94–103, 2006.

[12] Y. Ku and I. L. Jung, "Photocatalytic reduction of Cr(VI) in aqueous solutions by UV irradiation with the presence of titanium dioxide," *Water Research*, vol. 35, no. 1, pp. 135–142, 2001.

[13] R. A. Doong and W. H. Chang, "Photoassisted titanium dioxide mediated degradation of organophosphorus pesticides by hydrogen peroxide," *Journal of Photochemistry and Photobiology A*, vol. 107, no. 1–3, pp. 239–244, 1997.

[14] M. Kerzhentsev, C. Guillard, J. M. Herrmann, and P. Pichat, "Photocatalytic pollutant removal in water at room temperature: case study of the total degradation of the insecticide fenitrothion (phosphorothioic acid O,O-dimethyl-O-(3-methyl-4-nitro-phenyl) ester)," *Catalysis Today*, vol. 27, no. 1-2, pp. 215–220, 1996.

[15] C. S. Uyguner and M. Bekbolet, "Evaluation of humic acid, chromium (VI) and TiO_2 ternary system in relation to adsorptive interactions," *Applied Catalysis B*, vol. 49, no. 4, pp. 267–275, 2004.

[16] L. B. Khalil, W. E. Mourad, and M. W. Rophael, "Photocatalytic reduction of environmental pollutant Cr(VI) over some semiconductors under UV/visible light illumination," *Applied Catalysis B*, vol. 17, no. 3, pp. 267–273, 1998.

[17] E. N. Chirwa and Y. T. Wang, "Simultaneous chromium(VI) reduction and phenol degradation in an anaerobic consortium of bacteria," *Water Research*, vol. 34, no. 8, pp. 2376–2384, 2000.

[18] L. Wang, N. Wang, L. Zhu, H. Yu, and H. Tang, "Photocatalytic reduction of Cr(VI) over different TiO_2 photocatalysts and the effects of dissolved organic species," *Journal of Hazardous Materials*, vol. 152, no. 1, pp. 93–99, 2008.

[19] M. Fathizadeh, H. Fakhraee, and A. Aroujalian, "Decontamination of hexavalent chromium and tri-ethyl phosphate stimulants through photacatalytic oxidation," *International Journal of Environmental Science and Technology*, vol. 8, no. 4, pp. 863–871, 2011.

[20] C. R. Chenthamarakshan, K. Rajeshwar, and E. J. Wolfrum, "Heterogeneous photocatalytic reduction of Cr(VI) in UV-irradiated titania suspensions: effect of protons, ammonium ions, and other interfacial aspects," *Langmuir*, vol. 16, no. 6, pp. 2715–2721, 2000.

[21] U. Siemon, D. Bahnemann, J. J. Testa, D. Rodriguez, M. I. Litter, and N. Bruno, "Heterogeneous photocatalytic reactions comparing TiO_2 and Pt/TiO_2 ," *Journal of Photochemistry and Photobiology A*, vol. 148, no. 1, pp. 247–255, 2000.

Hindawi Publishing Corporation
Advances in Materials Science and Engineering
Volume 2012, Article ID 413638, 5 pages
doi:10.1155/2012/413638

Research Article

Photocatalytic Properties of Columnar Nanostructured TiO_2 Films Fabricated by Sputtering Ti and Subsequent Annealing

Zhengcao Li, Liping Xing, and Zhengjun Zhang

Advanced Materials Laboratory, Department of Materials Science and Engineering, Tsinghua University, Beijing 100084, China

Correspondence should be addressed to Zhengcao Li, zcli@tsinghua.edu.cn

Received 6 January 2012; Accepted 20 February 2012

Academic Editor: Guohua Jiang

Columnar nanostructured TiO_2 films were prepared by sputtering Ti target in pure argon with glancing angle deposition (GLAD) and subsequent annealing at 400°C for different hours in air. Compared with sputtering TiO_2 target directly, sputtering Ti target can be carried out under much lower base pressure, which contributes to obtaining discrete columnar nanostructures. In the present study, TiO_2 films obtained by annealing Ti films for different hours all kept discrete columnar structures as the Ti films deposited in GLAD regime. The longer the annealing time was, the better the phase transition accomplished from Ti to TiO_2 (a mixture of rutile and anatase), and the better it crystallized. In addition, those TiO_2 films performed photocatalytic decolorization effectively and showed a law changing over annealing time under UV light irradiation towards methyl orange, which demonstrated the potential applications for treatment of effluent.

1. Introduction

With the development of agriculture and industry, the global environmental problems are becoming more and more serious and have drawn more and more attention [1, 2]. The increasing environmental problems create a great demand for stable and environmentally friendly materials, which can perform efficient photocatalytic decomposition of hazardous substances before their emission to the environment. Photocatalytic degradation technique plays an important role to solve the organic pollution problems because it combines with solar energy and in perfect agreement with the requirement of sustainable processes development [3–5]. This technique can degrade organic pollutants into harmless inorganic substances such as CO_2 and H_2O under moderate conditions.

As an efficient photocatalyst, extensive research has been performed on titanium dioxide (TiO_2) along with its photocatalytic applications for effluent [6, 7]. Titanium dioxide (TiO_2) is nontoxic, chemically stabile and possesses a unique combination of optical and photochemical properties [8–10]. The mechanism of TiO_2 photocatalytic oxidation is to offer a highly reactive, nonspecific oxidant, namely hydroxyl radical ($^{\bullet}OH$) which is capable of destroying, wide range of organic pollutants nonselectively and quickly in wastewater [11–13].

A great amount of literature published for TiO_2 photocatalytic oxidation indicates the use of TiO_2 powders [14], but the TiO_2 powders have some practical problems such as immobilization and recycling which requires costly separation procedures after used. The columnar nanostructured TiO_2 film by GLAD [15, 16] in this paper has no problem with immobilization and recycling and has a relatively larger surface area compared with flat film which contributes to the photocatalytic efficiency.

This study investigated columnar nanostructured TiO_2 films annealed for different hours to get the law how the morphology, crystal structure, and photocatalytic properties change over annealing time at 400°C in air.

2. Experimental

Ti columnar structure was obtained by GLAD using magnetron sputtering and subsequently annealed under appropriate conditions to achieve TiO_2 columnar structure. And

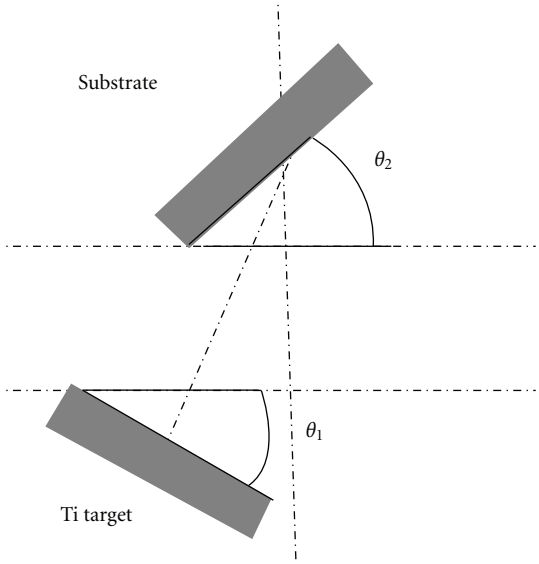

Figure 1: Schematic diagram of the GLAD technique in the magnetron sputtering system.

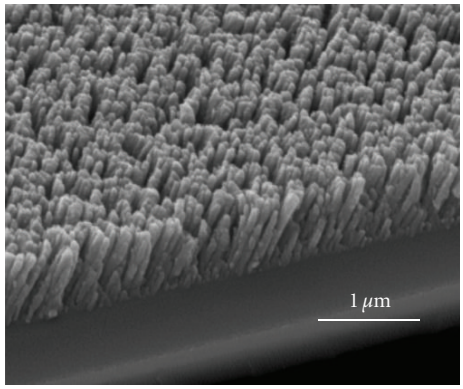

(a)

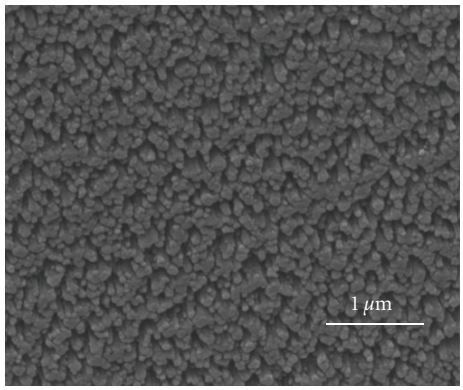

(b)

Figure 2: Cross-section and surface morphology of columnar nanostructured Ti film by GLAD.

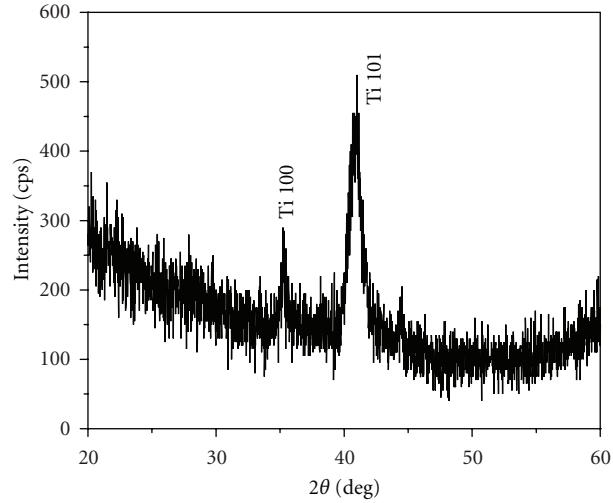

Figure 3: XRD spectra for columnar nanostructured Ti film by GLAD.

then some performance tests were carried out to get the morphology, crystal structure, and photocatalytic properties.

The main technology used in this paper to acquire columnar structure is glancing angle deposition (GLAD). The columnar microstructure exhibiting a high degree of porosity was obtained as a result of the shadow effect [17–20]. The schematic diagram of GLAD in the magnetron sputtering system is showed in Figure 1.

The sputtering of Ti in pure Ar was performed at low pressure (about 0.11 Pa). The distance between the Ti target and the Si substrate centers was about 11 cm. The purity of the Ti target was 99.99% (diameter of 60 mm and thickness of 3 mm). The Si substrates were 3-inchs monocrystalline ([100]) wafers with low resistivity (0.02 Ωcm). The deposition angle between the substrate normal and the incident flux was fixed at 80° ($\theta_1 = 25°$ and $\theta_2 = 55°$) for all depositions in the GLAD regime and was held constant in each experiment. Ar gas flow was kept 10 sccm during the deposition process which continued 90 minutes with a deposition power of 201.6 W.

Four groups of samples (columnar nanostructured Ti films) with size of 13 mm × 10 mm were annealed at 400°C in air for 1, 2, 3, and 4 hours, respectively, in quartz tube furnace to be oxidized and crystallized. Then columnar nanostructured films of a mixture of rutile and anatase were obtained.

Characterization was conducted using XRD, SEM, and UV-vis spectrophotometer.

XRD measurements were performed for structural characterization. The parameters of a diffractometer ($U = 45$ kV, $I = 200$ mA) were the same for all samples. The surface morphologies of the nanostructured films were observed by SEM. The photocatalytic activities of TiO_2 nanostructures were characterized by photocatalytic decomposition of methyl orange under UV light irradiation.

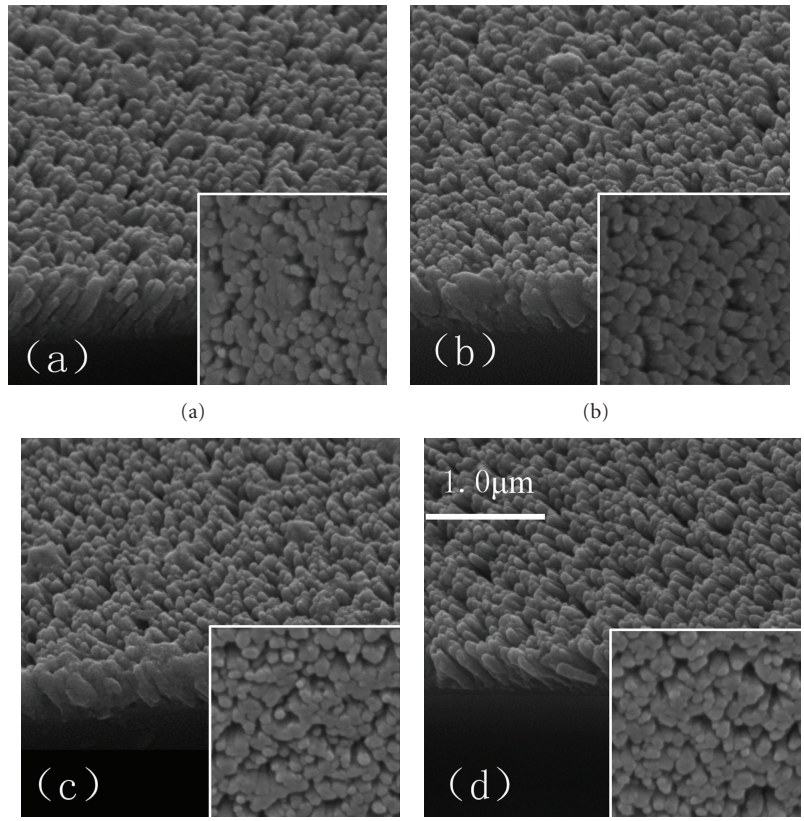

Figure 4: Cross-sections and surface morphologies of columnar nanostructured TiO_2 films after annealed at 400°C for (a) 1 hour, (b) 2 hours, (c) 3 hours and (d) 4 hours.

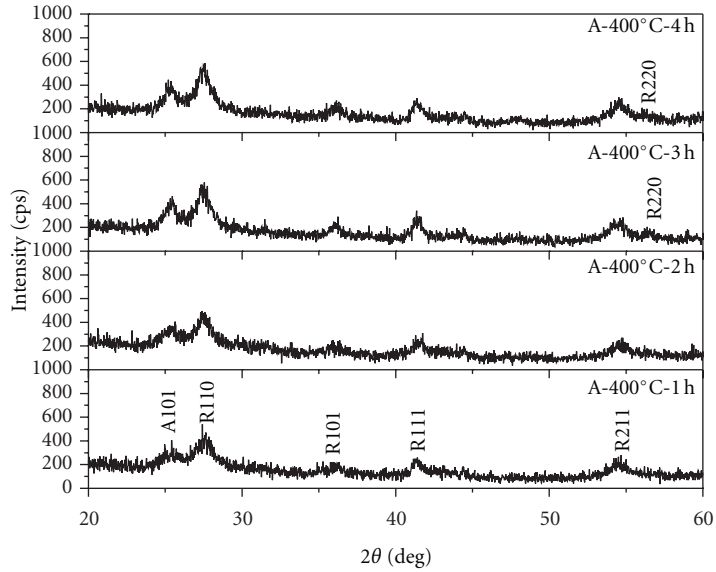

Figure 5: XRD spectra for columnar nanostructured TiO_2 films after annealed at 400°C for 1–4 hours.

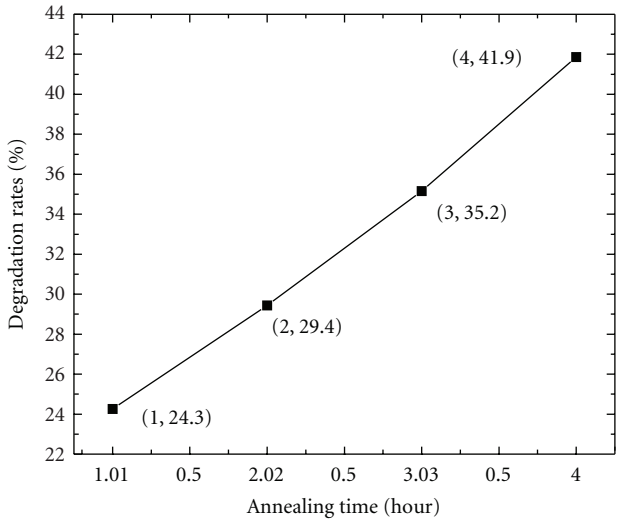

Figure 6: Transmittance spectra of methyl orange with sample annealed for (a) 4 hours, (b) 3 hours, (c) 2 hours, (d) 1 hour after 2-hour UV radiation, (e) without sample after 2-hour UV radiation and (f) without sample and no UV radiation.

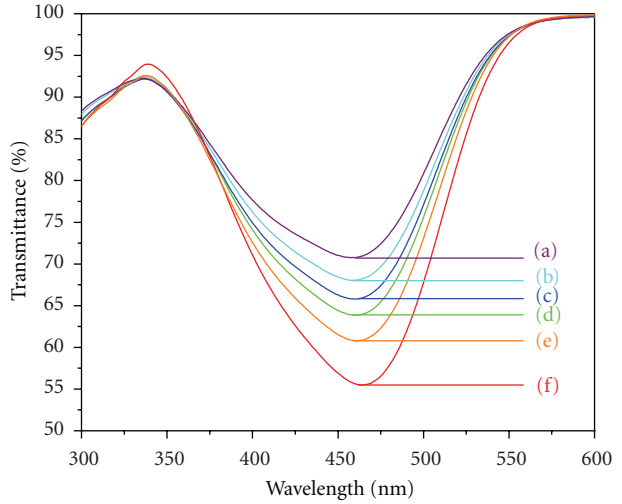

Figure 7: Degradation rates of methyl orange with TiO_2 sample annealed for different hours (1, 2, 3, and 4).

3. Results and Discussion

As shown in Figure 2, the Ti film by GLAD in the experiment has oblique aligned columnar nanostructure with a high degree of porosity and large surface area. XRD spectra in Figure 3 demonstrate that there is nothing else but Ti [20].

SEM images of the TiO_2 films annealed for 1, 2, 3, and 4 hours, respectively, are presented in Figure 4 (cross-sections and surface morphologies). There are almost no differences in discrete columnar morphologies between them [18, 21]. They all keep discrete columnar structures as the Ti films deposited by GLAD.

The diffraction patterns of the TiO_2 films show that peaks correspond to the known diffraction maxima of the anatase and rutile phase as marked in Figure 5. The columnar structure accomplished the phase transition from Ti to a mixture of rutile and anatase while keeping its discreetness [12]. XRD shows that the longer the annealing time is, the better it crystallizes. The average crystallite size D of rutile was calculated by Scherrer's equation using the full width at half-maximum of the XRD peaks of R (110). The sizes of the rutile grains in the TiO_2 films annealed for different hours are all about 10 nm.

Each TiO_2 sample was placed in the center of a small beaker with 5 mL diluted methyl orange (about 10 μmol/L) in it, and one beaker without TiO_2 sample but methyl orange was prepared for comparison. The photocatalytic degradation was performed under 500 W UV lamp for two hours. The concentration change of aqueous methyl orange is obtained from transmittance spectrum measured by a UV-vis spectrophotometer as shown in Figure 6.

Transmittances of methyl orange at 465 nm (a) with sample annealed for 4 hours after 2-hour UV radiation, (b) with sample annealed for 3 hours after 2-hour UV radiation, (c) with sample annealed for 2 hours after 2-hour UV radiation, (d) with sample annealed for 1 hour after 2-hour UV radiation, (e) without sample after 2-hour UV radiation, and (f) without sample and no UV radiation (origin methyl orange) are 71.0%, 68.3%, 66.0%, 64.0%, 61.0%, and 55.5%, respectively. According to Beer-Lambert law, absorbance and concentration of an absorbing species have a linear relationship, and the relation between A (absorbance) and T (transmittance) is $A = -\log T$; the degradation rates of methyl orange (a), (b), (c), (d), and (e) are 41.9%, 35.2%, 29.4%, 24.3%, and 16.0%, respectively [12]. The degradation rate increases from 16.0% to 41.9% due to the photocatalytic activity of TiO_2 nanostructures [13]. Furthermore, the degradation rate increases over annealing time as showed in Figure 7.

4. Conclusions

The columnar structure accomplished the phase transition from Ti to a mixture of rutile and anatase while keeping its discreteness after annealed at 400°C in air. The longer the annealing time is, the better the phase transition accomplishes from Ti to TiO_2 (a mixture of rutile and anatase), and the better it crystallizes. Those TiO_2 films all perform photocatalytic decolorization effectively and reusably under UV light irradiation towards methyl orange. The degradation rate increases with increasing annealing time and increases from 16.0% to 41.9% due to the photocatalytic activity of the obtained TiO_2 nanostructures.

Acknowledgments

The authors are grateful to the financial support by and the National Basic Research Program of China (973 program, 2010CB731600 and 2010CB832900) and the National Natural Science Foundation of China (61076003 and 61176003).

References

[1] L. W. Perelo, "Review: in situ and bioremediation of organic pollutants in aquatic sediments," *Journal of Hazardous Materials*, vol. 177, no. 1–3, pp. 81–89, 2010.

[2] J. R. Dominguez, J. Beltran, and O. Rodriguez, "Vis and UV photocatalytic detoxification methods (using TiO_2, TiO_2/H_2O_2, TiO_2/O_3, $TiO_2/S_2O_8^{2-}$," *Catalysis Today*, vol. 101, no. 3-4, pp. 389–395, 2005.

[3] P. Saritha, C. Aparna, V. Himabindu, and Y. Anjaneyulu, "Comparison of various advanced oxidation processes for the degradation of 4-chloro-2 nitrophenol," *Journal of Hazardous Materials*, vol. 149, no. 3, pp. 609–614, 2007.

[4] M. G. Neelavannan, M. Revathi, and C. Ahmed Basha, "Photocatalytic and electrochemical combined treatment of textile wash water," *Journal of Hazardous Materials*, vol. 149, no. 2, pp. 371–378, 2007.

[5] B. Mounir, M. N. Pons, O. Zahraa, A. Yaacoubi, and A. Benhammou, "Discoloration of a red cationic dye by supported TiO_2 photocatalysis," *Journal of Hazardous Materials*, vol. 148, no. 3, pp. 513–520, 2007.

[6] S. Malato, J. Blanco, A. Vidal, and C. Richter, "Photocatalysis with solar energy at a pilot-plant scale: an overview," *Applied Catalysis B*, vol. 37, no. 1, pp. 1–15, 2002.

[7] C. Yang, C. Gong, T. Peng, K. Deng, and L. Zan, "High photocatalytic degradation activity of the polyvinyl chloride (PVC)-vitamin C (VC)-TiO_2 nano-composite film," *Journal of Hazardous Materials*, vol. 178, no. 1–3, pp. 152–156, 2010.

[8] A. Fujishima, X. Zhang, and D. A. Tryk, "TiO_2 photocatalysis and related surface phenomena," *Surface Science Reports*, vol. 63, no. 12, pp. 515–582, 2008.

[9] P. K. Song, Y. Irie, and Y. Shigesato, "Crystallinity and photocatalytic activity of TiO_2 films deposited by reactive sputtering with radio frequency substrate bias," *Thin Solid Films*, vol. 496, no. 1, pp. 121–125, 2006.

[10] C. Burda, Y. Lou, X. Chen, A. C. S. Samia, J. Stout, and J. L. Gole, "Enhanced nitrogen doping in TiO_2 nanoparticles," *Nano Letters*, vol. 3, no. 8, pp. 1049–1051, 2003.

[11] C. Li and G. Song, "Photocatalytic degradation of organic pollutants and detection of chemical oxygen demand by fluorescence methods," *Sensors and Actuators B*, vol. 137, no. 2, pp. 432–436, 2009.

[12] Y. Pihosh, I. Turkevych, J. Ye et al., "Photocatalytic properties of TiO_2 nanostructures fabricated by means of glancing angle deposition and anodization," *Journal of the Electrochemical Society*, vol. 156, no. 9, pp. K160–K165, 2009.

[13] K. Ikeda, H. Sakai, R. Baba, K. Hashimoto, and A. Fujishima, "Photocatalytic reactions involving radical chain reactions using microelectrodes," *Journal of Physical Chemistry B*, vol. 101, no. 14, pp. 2617–2620, 1997.

[14] M. Farooq, I. A. Raja, and A. Pervez, "Photocatalytic degradation of TCE in water using TiO_2 catalyst," *Solar Energy*, vol. 83, no. 9, pp. 1527–1533, 2009.

[15] Q. Zhou, Z. C. Li, J. Ni, and Z. J. Zhang, "A simple model to describe the rule of glancing angle deposition," *Materials Transactions*, vol. 52, no. 3, pp. 469–473, 2011.

[16] Q. Zhou, Z. C. Li, Y. Yang, and Z. J. Zhang, "Arrays of aligned, single crystalline silver nanorods for trace amount detection," *Journal of Physics D*, vol. 41, no. 15, Article ID 152007, 2008.

[17] K. Robbie, J. C. Sit, and M. J. Brett, "Advanced techniques for glancing angle deposition," *Journal of Vacuum Science and Technology B*, vol. 16, no. 3, pp. 1115–1122, 1998.

[18] Y.-P. Zhao, D.-X. Ye, G.-C. Wang, and T.-M. Lu, "Designing nanostructures by glancing angle deposition," *Nanotubes and Nanowires*, vol. 5219, pp. 59–73, 2003.

[19] Y. Q. Wang, Z. C. Li, X. Sheng, and Z. J. Zhang, "Synthesis and optical properties of V_2 O_5 nanorods," *Journal of Chemical Physics*, vol. 126, no. 16, Article ID 164701, 2007.

[20] Z. C. Li, Y. Zhu, Q. Zhou, J. Ni, and Z. J. Zhang, "Photocatalytic properties of TiO_2 thin films obtained by glancing angle deposition," *Applied Surface Science*, vol. 258, no. 7, pp. 2766–2770, 2012.

[21] Z. C. Li, L. P. Xing, N. Zhang, Y. Yang, and Z. J. Zhang, "Preparation and photocatalytic property of TiO_2 columnar nanostructure films," *Materials Transactions*, vol. 52, no. 10, pp. 1939–1942, 2011.

Hindawi Publishing Corporation
Advances in Materials Science and Engineering
Volume 2012, Article ID 409379, 8 pages
doi:10.1155/2012/409379

Research Article

Preparation and Photocatalytic Activity of Magnetic $Fe_3O_4/SiO_2/TiO_2$ Composites

Rijing Wang,[1,2] Xiaohong Wang,[1,2] Xiaoguang Xi,[1,2] Ruanbing Hu,[1,2] and Guohua Jiang[1,2]

[1] *Department of Materials Engineering, College of Materials and Textile, Zhejiang Sci-Tech University, Hangzhou 310018, China*
[2] *Key Laboratory of Advanced Textile Materials and Manufacturing Technology (ATMT) of Ministry of Education, Zhejiang Sci-Tech University, Hangzhou 310018, China*

Correspondence should be addressed to Guohua Jiang, polymer_jiang@hotmail.com

Received 29 October 2011; Accepted 8 December 2011

Academic Editor: Qiang Yang

A simple sol-gel method was used to prepare magnetic $Fe_3O_4/SiO_2/TiO_2$ composites with core-shell structure. Fourier transform infrared spectroscopy (FT-IR), X-ray diffraction (XRD), field emission scanning electron microscopy (FE-SEM), and transmission electron microscopy (TEM) have been applied to investigate the structure and morphology of the resultant composites. The obtained composites showed excellent magnetism and higher photodegradation ability than pure TiO_2. The photocatalytic mechanism was also discussed. The magnetic composites should be extended to various potential applications, such as photodegradation, catalysis, separation, and purification processes.

1. Introduction

Currently, there has been great interest in the preparation of core-shell micro- and nanoparticles for their widespread potential applications in catalysis, chromatography separation, drug delivery, chemical reactors, and protection of environmentally sensitive materials [1–4]. Heterogeneous photocatalysis using semiconducting oxide catalysts is an effective way to purify wastewater or gas. TiO_2-based semiconductors have attracted considerable attention due to their high efficiency, good stability, availability, and nontoxicity [5–9]. In recent years, in order to enhance the photocatalytic activity, great efforts have been made to prepare ideal structure of TiO_2-based semiconductors [10–12].

Magnetic separation provides a very convenient approach for removing and recycling magnetic composites by applying an added magnetic field. The incorporation of Fe_3O_4 magnetic particles into TiO_2 matrix may block the aggregation of nanoparticles during renewal and can increase the durability of the catalysts [13, 14]. Moreover, such catalysts have a high surface area and well-defined pore size, which enhance their photocatalytic activity [15]. However, magnetic nanoparticles would inescapably encounter an hindrance when applied in practice due to the fact that a photocatalytic reaction is conducted in a suspension. It is not allowed to use magneton to agitate the mixed solutions. Therefore, in the experiment, Ar gas is purged so as to make the magnetic particles suspend in the methylene blue (MB) solution.

Many efforts have been made in the development of the design and preparation of magnetic core-shell microspheres. Ye et al. and Yu et al. reported the magnetic material/SiO_2 /TiO_2 composites with core-shell-shell structure [16, 17]. Their methods involve superparamagnetic Fe_3O_4 and γ-Fe_2O_3 with an inner layer of SiO_2 and outer layer of TiO_2 [18, 19]. Their resultant samples exhibit superior photodegradation ability and can be easily recycled by applying an external magnetic field. Zhou et al. reported the preparation of core-shell structure of Fe_3O_4/SiO_2 nanospheres via a modified inverse emulsion process [20]. Many methods have been applied to prepare composites with core-shell structure. However, it remains a great challenge to explore a feasible, easily controllable, and repeatable method for the preparation of core-shell nanostructure composites.

Nanosize TiO_2 exhibits superior photocatalytic activity compared to the common TiO_2 because of its rough surface and larger pore volumes. Herein, we directly use the Fe_3O_4 nanoparticles (a mean diameter of approximately 20 nm) as

the core of the composites, then a inner layer of SiO_2 and outer layer of TiO_2 were coated via a simple sol-gel process and a rapid combustion process. Silica coating is a necessary step to prepare core-shell structure because the hydrophobic Fe_3O_4 nanoparticles cannot be easily encapsulated in a TiO_2 shell [21]. Moreover, SiO_2 can be selectively etched onto the hollow magnetic/TiO_2 microspheres, allowing enough spaces for uploading some materials that can absorb polluted gas or wastewater. In the photocatalytic experiment, the pH of solution effect on the photocatalytic activity of catalyst was investigated and peroxide solution (30%) was added to enhance the catalyst activity through promoting the formation of hydroxyl radical and the reduced rate of interfacial electron transfer. This may open up new possibilities to synthesize core-shell structure for other composites and extend their applications.

2. Experimental Section

2.1. Materials and Reagents. Nanoiron (II, III) oxide (spherical, diameter 20 nm, 99.5%) was purchased from Shanghai Chemical Co., Ltd., China. Ammonia solution and isopropyl alcohol were obtained from Hangzhou High-Crystal Fine Chemical Co., Ltd., China. Tetraethoxysilane (TEOS) and tetrabutyltitanate (TBOT) were purchased from Tianjin Kermel Chemical Reagent Co., Ltd., China. Anhydrous ethanol was obtained from Hangzhou Changzheng Chemical Reagent Co., Ltd., China. Pure TiO_2 was purchased from Degussa Co. Ltd. All reagents were used without further purification. Deionized water was used in all experiments.

2.2. Preparation of Fe_3O_4/SiO_2 Nanospheres. The Fe_3O_4 nanoparticles (0.25 g) were ultrasonicated for 1 h to make them uniformly disperse in anhydrous ethanol (40 mL). Concentrated ammonium hydroxide (4.5 mL) was diluted to the above solution, and TEOS (0.8 mL) was quickly added under vigorous stirring. The solution was left to stir for 12 h. The product was collected by centrifugation and washed with anhydrous ethanol three times.

2.3. Preparation of Pomegranate-Like $Fe_3O_4/SiO_2/TiO_2$ Composite Microspheres. The resultant Fe_3O_4/SiO_2 nanocomposites were redispersed in anhydrous ethanol (40 mL). Subsequently, a proper amount of TBOT (1 mL) dissolved in isopropyl alcohol (8 mL) was introduced to the system dropwise, followed by heating the solution at about 70°C. The whole process was under vigorous stirring. After 12 h, the red brown precipitates were washed with deionized water and ethanol five times and dried in a vacuum oven at 60°C for 8 h. Finally, the products were calcined in air at 500°C for 2 h.

2.4. Characterization. X-ray diffraction (XRD) patterns were analyzed by X-ray diffractometer using Cu Kα radiation source at 35 kV, with a scan rate of 0.1° $2\theta\,s^{-1}$ in the 2θ range of 10–80°. The morphology and microstructure of products were characterized by ULTRA-55 field-emission scanning electron microscopy (FE-SEM) and JSM-2100 transmission electron microscopy (TEM) equipped with an energy dispersive X-ray spectrum (EDS, Inca Energy-200) at an accelerating voltage of 200 kV. Fourier transform infrared (FT-IR) spectra were recorded on a Nicolet 5700 spectrophotometer using KBr pellets for samples.

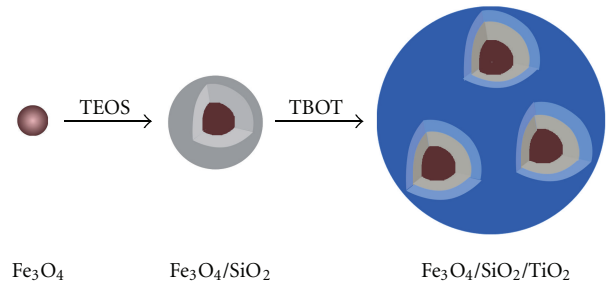

Scheme 1: The schematic process for preparing $Fe_3O_4/SiO_2/TiO_2$ composites.

2.5. Photocatalytic Activity Evaluation. The photocatalytic activity of $Fe_3O_4/SiO_2/TiO_2$ composites was investigated by the photodegradation of MB aqueous solution at ambient temperature. The photodegradation experiments were carried out in a closed box, of which UV radiation source is 100 W high-pressure mercury lamp, its wavelength range is 290−450 nm, and the peak intensity is 365 nm (Model OCRS-I, Kaifeng Hxsei Science Instrument Factory, China). No pure oxygen was supplied because it has enough oxygen for oxidation photodegradation under continuously stirring in atmosphere in previous experiment [22, 23]. The initial MB concentration (C_0) was 30 mg/L, the photocatalyst concentration was 0.5 g/L, and the pH of the solution was adjusted to 2, 7, and 10 with hydrochloric acid and sodium hydroxide solution. Before switching on the mercury, we passed Ar gas into the mixture solution of MB and photocatalyst in a dark condition for 30 min to achieve adsorption balance. The concentration of MB (C_t) was analyzed through JASCO V-570 UV/Vis/NiR spectrophotometer at $\lambda_{max} = 664$ nm. The concentration of MB (C_t) can be obtained by the following formula (where k is a constant):

$$A = k \times C. \tag{1}$$

Acetic acid (5 vol%, 5 mL) was also used to be photodegraded with $Fe_3O_4/SiO_2/TiO_2$ composites (20 mg) and pure TiO_2 using the aforementioned method. The amount of evolved CO_2 was determined by a gas chromatograph (GC, Agilent 6890).

3. Results and Discussion

The formation of $Fe_3O_4/SiO_2/TiO_2$ composites can be divided into two steps (Scheme 1). The first step is the hydrolyzation of TEOS on the Fe_3O_4 nanoparticles by the classical Stöber method; the silica layer can be easily coated on the surface of Fe_3O_4 nanoparticles. Some Fe_3O_4/SiO_2 nanoparticles would be aggregated, and the hydrolyzation of TBOT on the Fe_3O_4/SiO_2 composites resulted in the formation of pomegranate-like structure.

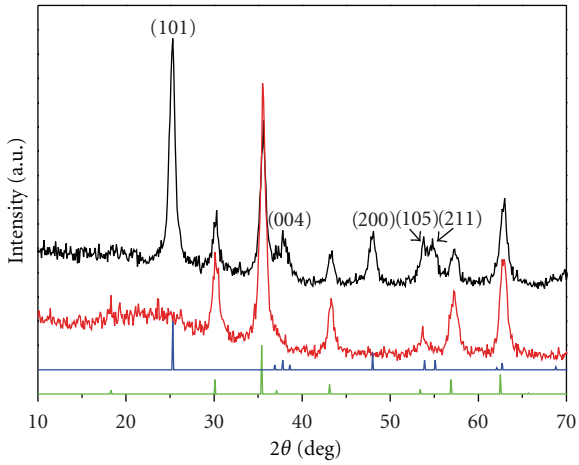

(A) Fe_3O_4/SiO_2 (C) JCPDS 19-0629
(B) $Fe_3O_4/SiO_2/TiO_2$ (D) JCPDS 21-1272

Figure 1: XRD pattern of Fe_3O_4/SiO_2 (A) and $Fe_3O_4/SiO_2/TiO_2$ composites (B).

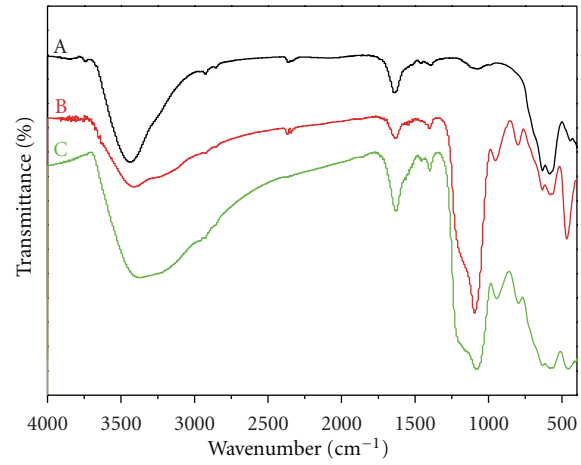

(A) Fe_3O_4
(B) Fe_3O_4/SiO_2
(C) $Fe_3O_4/SiO_2/TiO_2$

Figure 2: FT-IR spectra of Fe_3O_4 (A), Fe_3O_4/SiO_2 (B), and $Fe_3O_4/SiO_2/TiO_2$ composites (C).

The Fe_3O_4/SiO_2 and $Fe_3O_4/SiO_2/TiO_2$ composites were characterized by XRD. As shown in Figure 1(A), all peaks can be indexed as the magnetite phase of Fe_3O_4 (JCPDS 19-0629). No characteristic peaks of SiO_2 were detected, indicating that the SiO_2 was amorphous. In contrast to Figure 1(A), the successful TiO_2 coating was confirmed by the presence of the new peaks (Figure 1(B)). The reduction of Fe_3O_4 peaks also confirmed the successful TiO_2 coating. The as-prepared samples displayed good crystallinity; and the TiO_2 peaks can be ascribed to the (101), (004), (200), (105), and (211) planes of anatase phase (JCPDS 21-1272). According to the Scherrer equation,

$$D = \frac{0.89\lambda}{(\gamma \cos\theta)}, \quad (2)$$

where D is the average crystallite size, the factor 0.89 is characteristic of spherical objects, λ is the X-ray wavelength, γ and θ are the full width at half-maximum and diffraction angle of an observed peak, respectively. The primary crystallite size calculated from the (101) peak of the XRD pattern was about 12.64 nm.

FT-IR was used to characterize the composition and structure of the Fe_3O_4, Fe_3O_4/SiO_2, and $Fe_3O_4/SiO_2/TiO_2$ composites. As shown in Figure 2, the $Fe_3O_4/SiO_2/TiO_2$ composites possess more signals than Fe_3O_4. It has been reported that the signal at the wave number around 800 cm^{-1} corresponds to the symmetric vibration of Si–O–Si, 1080 cm^{-1} for asymmetric stretching vibration of Si–O–Si, and 940–960 cm^{-1} for Si–O–Ti vibration and 500–900 cm^{-1} originates from Ti–O–Ti [24, 25]. Silica presence as an amorphous phase was confirmed by combining the results of FT-IR and XRD. The presence of water is evidenced by the appearance of the bending mode at 1630 cm^{-1} and the stretching mode at 3370 cm^{-1}. This surface hydroxylation is advantageous for the photocatalytic activity of $Fe_3O_4/SiO_2/TiO_2$ microspheres because it provides higher capacity for oxygen adsorption [26].

The morphology and structure of the as-prepared samples were investigated by field emission scanning electron microscopy (FE-SEM). Figure 3(a) shows that the Fe_3O_4 nanoparticles are of a diameter of 20 ± 2 nm. They prefer to gather together due to their small size and magnetic. The grape-like Fe_3O_4/SiO_2 nanospheres with a diameter of 25 ± 2 nm are shown in Figure 3(b). This indicated that SiO_2 was successfully coated on the Fe_3O_4 nanoparticles. Figures 3(c) and 3(d) present typical FE-SEM images of as-prepared $Fe_3O_4/SiO_2/TiO_2$ composites. These images indicate that the surfaces of $Fe_3O_4/SiO_2/TiO_2$ microspheres are rough and porous, which favor enhancing the photocatalytic activity [27]. A large number of Fe_3O_4/SiO_2 nanospheres are encapsulated in the core of TiO_2 shell, forming the pomegranate-like structure, which can make the dyes better contact with the catalysts so as to achieve the purpose of degradation [28].

The morphology and structure of the resultant samples were further investigated by transmission electron microscopy (TEM) (Figure 4). As expected, the Fe_3O_4/SiO_2 nanospheres were composed of aggregated spherical particles with sizes around 25 nm. Moreover, a large number of nanoparticles are encapsulated in the SiO_2 layer (Figure 4(a)). In contrast to the morphology of Fe_3O_4/SiO_2 nanoparticles, Figure 4(b) clearly displays that TiO_2 was successfully coated on Fe_3O_4/SiO_2 nanoparticles. The EDS pattern (Figure 5) taken from this area shows the presence of only Fe, Si, Ti, and O elements.

Magnetic separation provides a very convenient approach for removing and recycling magnetic catalysts. The magnetism of $Fe_3O_4/SiO_2/TiO_2$ composites was confirmed by Figure 6, and the $Fe_3O_4/SiO_2/TiO_2$ composites were tested in water by placing a magnet near the glass bottle. The red brown particles can be attracted toward the magnet

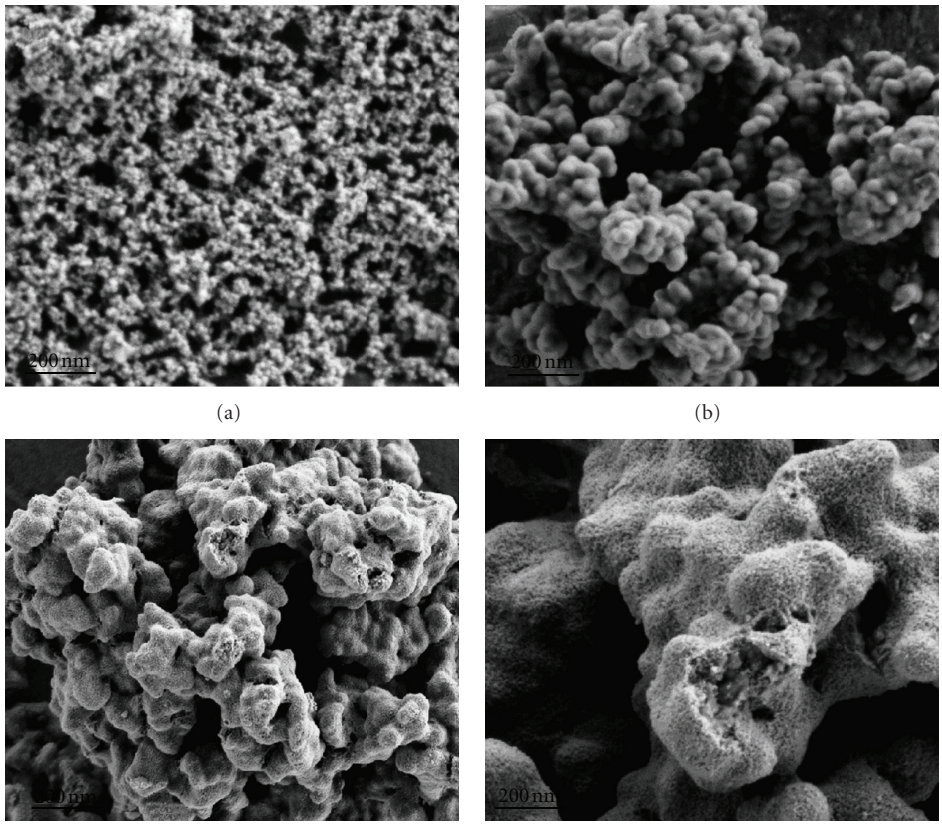

Figure 3: FE-SEM images of Fe_3O_4 (a) and Fe_3O_4/SiO_2 (b) $Fe_3O_4/SiO_2/TiO_2$ composite microspheres (c, d).

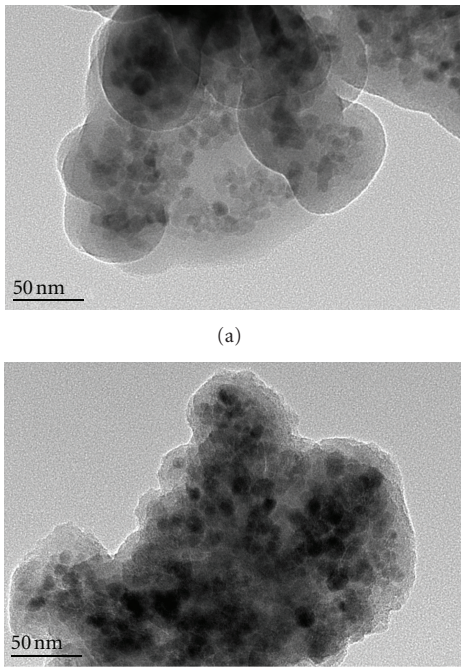

Figure 4: TEM images of Fe_3O_4/SiO_2 (a) and $Fe_3O_4/SiO_2/TiO_2$ composite microspheres (b).

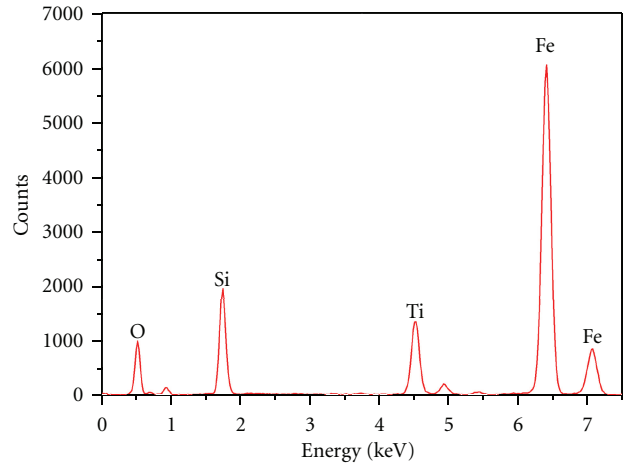

Figure 5: EDS pattern of $Fe_3O_4/SiO_2/TiO_2$ composites calcined at 500°C for 2 h.

with time increasing, and the $Fe_3O_4/SiO_2/TiO_2$ almost totally attracted after 5 min, leaving a clear solution. So the as-prepared samples can be easily recycled after the achievement of photocatalytic process.

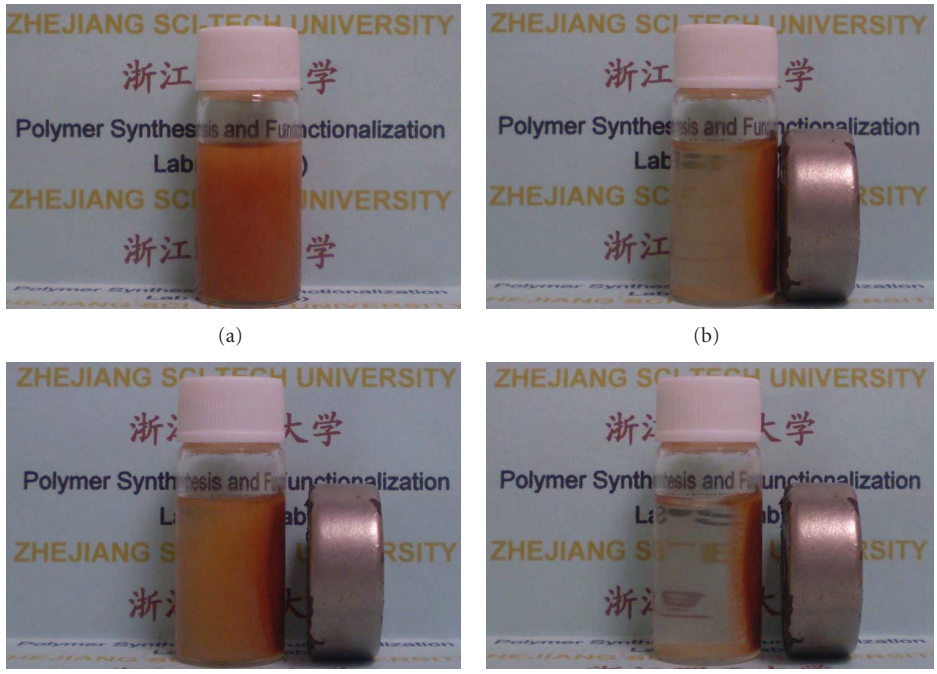

Figure 6: Digital illumination photographs of $Fe_3O_4/SiO_2/TiO_2$ composites separated from solution by applying an added magnet ((a) 0 min, (b) 1 min, (c) 2 min, and (d) 5 min).

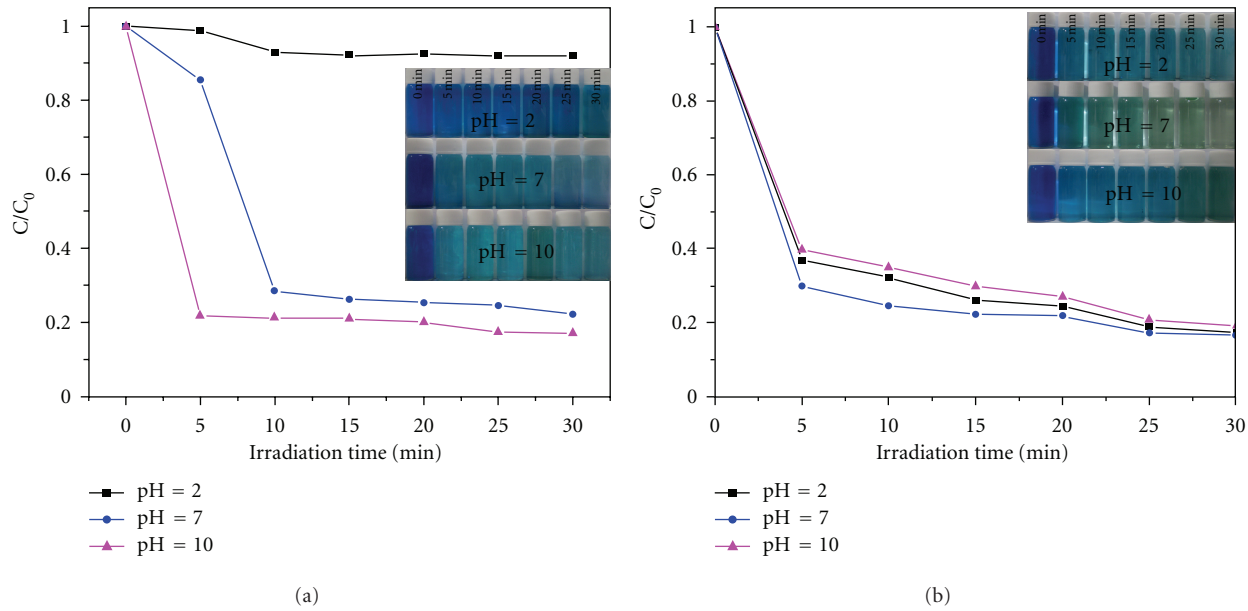

Figure 7: Photodegradation efficiency of $Fe_3O_4/SiO_2/TiO_2$ composite microspheres and digital illumination photographs at pH 2, 7, and 10 ((a) with 1 mL H_2O; (b) with 1 mL H_2O_2).

Figure 7 depicts the photocatalytic activity of $Fe_3O_4/SiO_2/TiO_2$ composites and shows the digital illumination photographs of MB aqueous solution under UV light irradiation at different pH values with H_2O_2 or without. In the experiment, we used the deionized water as the blank, comparing with H_2O_2 to ensure only a variable. Figure 7(a) shows that the rate of photodegradation of MB was higher at the neutral and alkaline environment. 78% photodegradation of MB solution (pH = 10) was observed after 5 min under UV irradiation. However, in the acidic condition, only 8.5% of MB has been photodegraded after 30 min. As shown in the digital illumination photographs of MB aqueous solution under UV light irradiation at different pH values. The color of MB solution fades gradually with irradiation time at

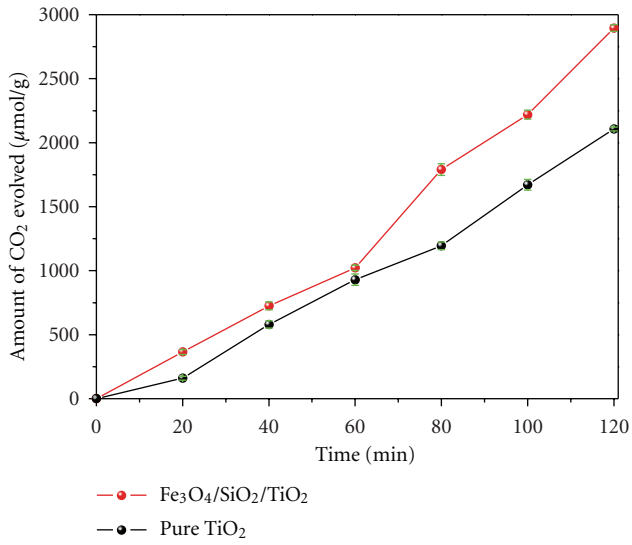

Figure 8: Relationship between the amount of CO_2 evolved and irradiation time for photocatalytic degradation of acetic acid aqueous solution.

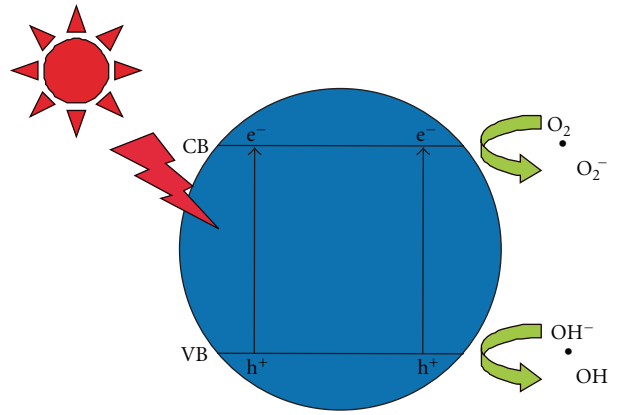

Scheme 2: The scheme of photocatalytic mechanism of $Fe_3O_4/SiO_2/TiO_2$ composite microspheres.

pH = 7 and 10, but with no distinct change of the color at pH = 2. This is because the pH influenced the adsorption property of organic compounds and their dissociating state in solution. The surface charge properties of TiO_2 were also changed with the changes in pH value due to amphoteric behavior of semiconducting TiO_2 [29]. It is interesting to see from Figure 7(b) that photodegradation efficiency of MB at different pH values with H_2O_2 can reach 60% after 5 min under UV irradiation. H_2O_2 enhanced the photodegradation ability attributed to its electron acceptor behavior, which reacted with conduction band electrons to generate hydroxyl radicals. The point of zero charge (pzc) for titanium dioxide is at pH 6.5. The TiO_2 surface is positively charged in acidic solution and negatively charged in basic solution [30]. Since MB is a cationic dye, it is conceivable that, at higher pH value, its adsorption is favored on a negatively charged surface.

In order to demonstrate the photocatalytic activity of $Fe_3O_4/SiO_2/TiO_2$ composites, acetic acid was selected as a model organic acid. As shown in Figure 8, the amount of CO_2 evolution increases with irradiation time for pure TiO_2 and $Fe_3O_4/SiO_2/TiO_2$. However, in case of $Fe_3O_4/SiO_2/TiO_2$, the yield rate of CO_2 reaches about $1448.05 \pm 6.25\,\mu\text{mol}\,\text{h}^{-1}\,\text{g}^{-1}$, which is higher than pure TiO_2 ($1053.12 \pm 7.23\,\mu\text{mol}\,\text{h}^{-1}\,\text{g}^{-1}$) for 2 h. The higher CO_2 evolution rate for $Fe_3O_4/SiO_2/TiO_2$ sample may be attributed to rough and porous surface of $Fe_3O_4/SiO_2/TiO_2$ composites, which enhances the photocatalytic activity by facilitating the access to the reactive TiO_2.

The schematic illustration of the charge transfer by $Fe_3O_4/SiO_2/TiO_2$ composites is summarized in Scheme 2. Photoexcitation of the $Fe_3O_4/SiO_2/TiO_2$ composites likely results in charge separation to form electrons and holes (3) [31]. Photo-generated electrons can directly react with the absorbed O_2 molecules to form $\cdot O_2^-$ active species (4). Photogenerated electrons also capture H_2O_2 molecules to produce $\cdot$OH and OH^- (5). The resultant $\cdot O_2^-$ can react with H_2O_2 to form $\cdot$OH and OH^- (6). The obtained OH^- can react with photogenerated holes to generate the hydroxyl free radical $\cdot$OH (7) [32]. Both $\cdot O_2^-$ and $\cdot$OH can photodegrade the MB solution:

$$TiO_2 + h\nu \longrightarrow TiO_2 + h^+ + e^- \quad (3)$$

$$O_2 + e^- \longrightarrow O_2^- \quad (4)$$

$$H_2O_2 + e^- \longrightarrow \bullet OH + OH^- \quad (5)$$

$$H_2O_2 + O_2^- \longrightarrow \bullet OH + OH^- \quad (6)$$

$$OH^- + h^+ \longrightarrow \bullet OH. \quad (7)$$

H_2O_2 enhanced photodegradation ability attributed to its electron acceptor behavior, which reacted with conduction band electrons to generate hydroxyl radicals.

4. Conclusion

In summary, the magnetic $Fe_3O_4/SiO_2/TiO_2$ composites have been prepared by a simple sol-gel method. The morphology and structure of the resultant samples were characterized by FT-IR, XRD, FE-SEM, and TEM. The $Fe_3O_4/SiO_2/TiO_2$ composites show excellent magnetism and higher photocatalytic activity than pure TiO_2 attributed to rough and porous surface of $Fe_3O_4/SiO_2/TiO_2$ composites, which enhances the photocatalytic activity by facilitating the access to the reactive TiO_2. The photocatalytic mechanism was also discussed. The magnetic $Fe_3O_4/SiO_2/TiO_2$ composites should be extended to various potential applications, such as photocatalysis, separation, and purification processes.

Acknowledgments

This work was financially supported by the Qianjiang Talents Project of Zhejiang Province (2010R10023), the Scientific Research Foundation for the Returned Overseas Chinese Scholars, the State Education Ministry (1001603-C), the Natural Science Foundation of Zhejiang Province

(Y4100045, Y4080392, R210101054), Foundation of Zhejiang Province New Textile Research and Development Emphasised Laboratory (2009FZD001), the Key Bidding Project of Zhejiang Provincial Key Lab of Fiber Materials and Manufacturing Technology, Zhejiang Sci-Tech University (S2010002), and the Program for Changjiang Scholars and Innovative Research Team in University (PCSIRT: 0654).

References

[1] F. Caruso, R. A. Caruso, and H. Möhwald, "Nanoengineering of inorganic and hybrid hollow spheres by colloidal templating," *Science*, vol. 282, no. 5391, pp. 1111–1114, 1998.

[2] R. A. Caruso, A. Susha, and F. Caruso, "Multilayered titania, silica, and Laponite nanoparticle coatings on polystyrene colloidal templates and resulting inorganic hollow spheres," *Chemistry of Materials*, vol. 13, no. 2, pp. 400–409, 2001.

[3] F. Caruso, X. Shi, R. A. Caruso, and A. Susha, "Hollow titania spheres from layered precursor deposition on sacrificial colloidal core particles," *Advanced Materials*, vol. 13, no. 10, pp. 740–744, 2001.

[4] G. Li, Q. Shi, S. J. Yuan, K. G. Neoh, E. T. Kang, and X. Yang, "Alternating silica/polymer multilayer hybrid microspheres templates for double-shelled polymer and inorganic hollow microstructures," *Chemistry of Materials*, vol. 22, no. 4, pp. 1309–1317, 2010.

[5] J. M. Herrmann, "Heterogeneous photocatalysis: fundamentals and applications to the removal of various types of aqueous pollutants," *Catalysis Today*, vol. 53, no. 1, pp. 115–129, 1999.

[6] Z. Xu and J. Yu, "Visible-light-induced photoelectrochemical behaviors of Fe-modified TiO_2 nanotube arrays," *Nanoscale*, vol. 3, no. 8, pp. 3138–3144, 2011.

[7] H. Li, Z. Bian, J. Zhu, Y. Huo, H. Li, and Y. Lu, "Mesoporous Au/TiO_2 nanocomposites with enhanced photocatalytic activity," *Journal of the American Chemical Society*, vol. 129, no. 15, pp. 4538–4539, 2007.

[8] H. Q. Wang, Z. B. Wu, and Y. Liu, "A simple two-step template approach for preparing carbon-doped mesoporous TiO_2 hollow microspheres," *Journal of Physical Chemistry C*, vol. 113, no. 30, pp. 13317–13324, 2009.

[9] X. Chen and S. S. Mao, "Titanium dioxide nanomaterials: synthesis, properties, modifications and applications," *Chemical Reviews*, vol. 107, no. 7, pp. 2891–2959, 2007.

[10] J. C. Lee, T. G. Kim, W. Lee, S. H. Han, and Y. M. Sung, "Growth of CdS nanorod-coated TiO_2 nanowires on conductive glass for photovoltaic applications," *Crystal Growth and Design*, vol. 9, no. 10, pp. 4519–4523, 2009.

[11] R. A. Lucky, R. Sui, J. M. H. Lo, and P. A. Charpentier, "Effect of solvent on the crystal growth of one-dimensional $ZrO_2 \cdot TiO_2$ nanostructures," *Crystal Growth and Design*, vol. 10, no. 4, pp. 1598–1604, 2010.

[12] S. Xuan, W. Jiang, X. Gong, Y. Hu, and Z. Chen, "Magnetically separable Fe_3O_4/TiO_2 hollow spheres: fabrication and photocatalytic activity," *Journal of Physical Chemistry C*, vol. 113, no. 2, pp. 553–558, 2009.

[13] W. Cheng, K. Tang, Y. Qi, J. Sheng, and Z. Liu, "One-step synthesis of superparamagnetic monodisperse porous Fe_3O_4 hollow and core-shell spheres," *Journal of Materials Chemistry*, vol. 20, no. 9, pp. 1799–1805, 2010.

[14] Z. Liu, H. Bai, and D. D. Sun, "Facile fabrication of porous chitosan/TiO_2/Fe_3O_4 microspheres with multifunction for water purifications," *New Journal of Chemistry*, vol. 35, no. 1, pp. 137–140, 2011.

[15] M. Shokouhimehr, Y. Piao, J. Kim, Y. Jang, and T. Hyeon, "A magnetically recyclable nanocomposite catalyst for olefin epoxidation," *Angewandte Chemie—International Edition*, vol. 46, no. 37, pp. 7039–7043, 2007.

[16] M. M. Ye, Q. Zhang, Y. X. Hu et al., "Magnetically recoverable core-shell nanocomposites with enhanced photocatalytic activity," *Chemistry—A European Journal*, vol. 16, no. 21, pp. 6243–6250, 2010.

[17] X. Yu, S. Liu, and J. Yu, "Superparamagnetic γ-$Fe_2O_3/SiO_2/TiO_2$ composite microspheres with superior photocatalytic properties," *Applied Catalysis B*, vol. 104, no. 1-2, pp. 12–20, 2011.

[18] W. Stöber, A. Fink, and E. Bohn, "Controlled growth of monodisperse silica spheres in the micron size range," *Journal of Colloid And Interface Science*, vol. 26, no. 1, pp. 62–69, 1968.

[19] J. W. Lee, M. R. Othman, Y. Eom, T. G. Lee, W. S. Kim, and J. Kim, "The effects of sonification and TiO_2 deposition on the micro-characteristics of the thermally treated SiO_2/TiO_2 spherical core-shell particles for photo-catalysis of methyl orange," *Microporous and Mesoporous Materials*, vol. 116, no. 1-3, pp. 561–568, 2008.

[20] J. Zhou, L. Meng, Q. Lu, J. Fu, and X. Huang, "Superparamagnetic submicro-megranates: Fe_3O_4 nanoparticles coated with highly cross-linked organic/inorganic hybrids," *Chemical Communications*, no. 42, pp. 6370–6372, 2009.

[21] C. Hui, C. Shen, J. Tian et al., "Core-shell Fe_3O_4/SiO_2 nanoparticles synthesized with well-dispersed hydrophilic Fe_3O_4 seeds," *Nanoscale*, vol. 3, no. 2, pp. 701–705, 2011.

[22] Y. Chen, K. Wang, and L. Lou, "Photodegradation of dye pollutants on silica gel supported TiO_2 particles under visible light irradiation," *Journal of Photochemistry and Photobiology A*, vol. 163, no. 1-2, pp. 281–287, 2004.

[23] G. Jiang, X. Zheng, Y. Wang, T. Li, and X. Sun, "Photo-degradation of methylene blue by multi-walled carbon nanotubes/TiO_2 composites," *Powder Technology*, vol. 207, no. 1–3, pp. 465–469, 2011.

[24] K. Y. Jung and S. B. Park, "Enhanced photoactivity of silica-embedded titania particles prepared by sol-gel process for the decomposition of trichloroethylene," *Applied Catalysis B*, vol. 25, no. 4, pp. 249–256, 2000.

[25] Z. Ding, G. Q. Lu, and P. F. Greenfield, "Role of the crystallite phase of TiO_2 in heterogeneous photocatalysis for phenol oxidation in water," *Journal of Physical Chemistry B*, vol. 104, no. 19, pp. 4815–4820, 2000.

[26] Z. Liu, X. Quan, H. Fu, X. Li, and K. Yang, "Effect of embedded-silica on microstructure and photocatalytic activity of titania prepared by ultrasound-assisted hydrolysis," *Applied Catalysis B*, vol. 52, no. 1, pp. 33–40, 2004.

[27] J. Yu, X. Yu, B. Huang, X. Zhang, and Y. Dai, "Hydrothermal synthesis and visible-light photocatalytic activity of novel cage-like ferric oxide hollow spheres," *Crystal Growth and Design*, vol. 9, no. 3, pp. 1474–1480, 2009.

[28] J. Yu, L. Zhang, B. Cheng, and Y. Su, "Hydrothermal preparation and photocatalytic activity of hierarchically sponge-like macro-/mesoporous Titania," *Journal of Physical Chemistry C*, vol. 111, no. 28, pp. 10582–10589, 2007.

[29] G. Jiang, R. Wang, H. Jin et al., "Preparation of Cu_2O/TiO_2 composite porous carbon microspheres as efficient visible light-responsive photocatalysts," *Powder Technology*, vol. 212, no. 1, pp. 284–288, 2011.

[30] R. J. Wang, G. H. Jiang, Y. W. Ding et al., "Photocatalytic activity of heterostructures based on TiO_2 and halloysite nanotubes," *ACS Applied Materials and Interfaces*, vol. 3, no. 10, pp. 4154–4158, 2011.

[31] L. Cao, S. Sahu, P. Anilkumar et al., "Carbon nanoparticles as visible-light photocatalysts for efficient CO_2 conversion and beyond," *Journal of the American Chemical Society*, vol. 133, no. 13, pp. 4754–4757, 2011.

[32] Q. Xiang, J. Yu, and P. K. Wong, "Quantitative characterization of hydroxyl radicals produced by various photocatalysts," *Journal of Colloid and Interface Science*, vol. 357, no. 1, pp. 163–167, 2011.

Hindawi Publishing Corporation
Advances in Materials Science and Engineering
Volume 2012, Article ID 348927, 5 pages
doi:10.1155/2012/348927

Research Article

Synthesis and Characterization of Fe-N-S-tri-Doped TiO_2 Photocatalyst and Its Enhanced Visible Light Photocatalytic Activity

Biying Li,[1] Xiuwen Cheng,[2,3] Xiujuan Yu,[2] Lei Yan,[1] and Zipeng Xing[2]

[1] *College of Resource and Environment, Northeast Agricultural University, Wood Sreet 59, Xiangfang District, Harbin 150030, China*
[2] *Department of Environmental Science and Engineering, Heilongjiang University, Xuefu Road 74, Nangang District, Harbin 150080, China*
[3] *State Key Laboratory of Urban Water Resources and Environment (SKLUWRE), Department of Environmental Science and Engineering Harbin Institute of Technology, Huanghe Road 73, Nangang District, Harbin 150090, China*

Correspondence should be addressed to Xiujuan Yu, yuxjuan@hit.edu.cn

Received 19 October 2011; Accepted 8 December 2011

Academic Editor: Guohua Jiang

Fe-N-S-tri-doped TiO_2 photocatalysts were synthesized by one step in the presence of ammonium ferrous sulfate. The resulting materials were characterized by X-ray diffraction (XRD), X-ray photoelectron spectroscopy (XPS), and ultraviolet-visible diffuse reflection spectrum (UV-Vis DRS). XPS analysis indicated that Fe (III) and S^{6+} were incorporated into the lattice of TiO_2 through substituting titanium atoms, and N might coexist in the forms of substitutional N (O-Ti-N) and interstitial N (Ti-O-N) in tridoped TiO_2. XRD results showed that tri-doping with Fe, N, and S elements could effectively retard the phase transformation of TiO_2 from anatase to rutile and growth of crystallite size. DRS results revealed that the light absorbance edge of TiO_2 in visible region was greatly improved by tri-doping with Fe, N, and S elements. Further, the photocatalytic activity of the as-synthesized samples was evaluated by the degradation of phenol under visible light irradiation. It was found that Fe-N-S-tri-doped TiO_2 catalyst exhibited higher visible light photocatalytic activity than that of pure TiO_2 and P25 TiO_2, which was mainly attributed to the small crystallite size, intense light absorbance in visible region, and narrow bandgap energy.

1. Introduction

Since the compounds in wastewater were treated by photocatalytic oxidation in 1976 by Carey et al. [1], TiO_2 nanomaterial has been considered as a promising photocatalyst in the degradation of organic or inorganic pollutants due to its inexpensiveness, nontoxicity, photostability and strong oxidation ability. However, TiO_2 can only be excited by UV light, which only occupies a small part of the solar spectrum [2]. In order to improve the utilization of solar energy, a great deal of efforts has been made, which include dye sensitization, coupling of TiO_2 with a narrow band gap semiconductor, noble metal deposition, and doping of TiO_2 with foreign ions [3–6]. Among which, doping of TiO_2 with foreign ions has been considered as an effective and feasible approach to enhance the photoresponse and photocatalytic activity. Very recently, it was reported that the doping of TiO_2 with two or three elements could further improve the light absorbance in visible region and photocatalytic activity [7–12]. From then on, many attempts have been carried out.

In this study, Fe-N-S-tridoped TiO_2 photocatalysts were synthesized by one step in the presence of ammonium ferrous sulfate. Fe (III) and S^{6+} were incorporated into the lattice of TiO_2 through substituting titanium atoms, and N might coexist in the forms of substitutional N (O-Ti-N) and interstitial N (Ti-O-N) in tridoped TiO_2. Fe-N-S-tridoped TiO_2 catalyst exhibited a higher visible light photocatalytic activity for the degradation of RhB than that of pure TiO_2 and P25 TiO_2.

2. Experimental

2.1. Synthesis of Materials. The Fe-N-S-tridoped TiO_2 photocatalysts were synthesized through sol-gel method in the

presence of ammonium ferrous sulfate. Firstly, 10 mL of tetrabutyl titanate was mixed with 40 mL of absolute ethanol. Then, the titanate-ethanol solution was added dropwise into another solution, which consisted of 10 mL of absolute ethanol, 12 mL of dilute nitric acid (1 : 5, volume ratio between concentration nitric acid and deionized water) and the desired amount of ammonium ferrous sulfate under vigorously stirring to carry out hydrolysis. Subsequently, the mixed solution was continuously stirred for 2 h at room temperature. After the resulting sol was aged for 6 h and dried for 36 h at 80°C, the TiO_2 precursor was obtained. Finally, Fe-N-S-tridoped TiO_2 catalysts were successfully obtained by calcining the TiO_2 precursor at 350°C for 4 h in an oven with a heating rate of $3°C \cdot min^{-1}$. For comparison, pure TiO_2 was synthesized under otherwise the identical conditions in the absence of ammonium ferrous sulfate.

2.2. Characterization of Materials. X-ray powder diffraction (XRD) patterns were performed on a Bruker D8 advance powder X-ray diffractometer with Cu Kα radiation (λ = 0.15418 nm). X-ray photoelectron spectroscopy (XPS) conducted using a PHI-5700 ESCA system was employed to characterize the chemical states of tridoped ferrum, nitrogen, and sulfur atoms in the as-synthesized samples. All the binding energies were calibrated with respect to the signal for adventitious carbon (binding energy = 284.6 eV). The UV-visible diffuse reflectance spectra (DRS) of the samples were recorded on a UV-2550 UV-visible spectrophotometer with an integrating sphere attachment. The analyzed wavelength range was 300~700 nm, and $BaSO_4$ was used as the reflectance standard.

2.3. Evaluation of Photocatalytic Activity. The photodegradation experiments were performed in a self-made photoreactor containing 20 mL of 50 $mg \cdot L^{-1}$ phenol and 20 mg of catalysts. A 350 W xenon arc lamp equipped with an UV cutoff filter (λ > 420 nm) was used as the visible light source. Prior to irradiation, the suspension was stirred in the dark for 60 min to establish the equilibrium of adsorption-desorption. At given time intervals, the phenol concentration was analyzed using the colorimetric method of 4-aminoantipyrineby with an UV-visible spectrophotometer (UV-2550) at the wavelength of 510 nm after centrifugation and filtration.

3. Results and Discussion

3.1. XRD Analysis. Figure 1 showed the XRD patterns of the as-synthesized TiO_2 samples. It can be seen that pure TiO_2 contained anatase (JCPDS, no. 21–1272), rutile (JCPDS, no. 21–1276) and brookite (JCPDS, no. 29–1360) with anatase phase in the majority according to their peak intensities. However, Fe-N-S-tridoped-TiO_2 consisted of anatase as the unique phase (JCPDS, no. 21–1272). Generally, brookite is a transitional phase from anatase to rutile during the calcinating process. Thus, it can be induced that tri-doping with Fe, N, and S elements could effectively retard the phase transformation of TiO_2 from anatase to rutile. In addition,

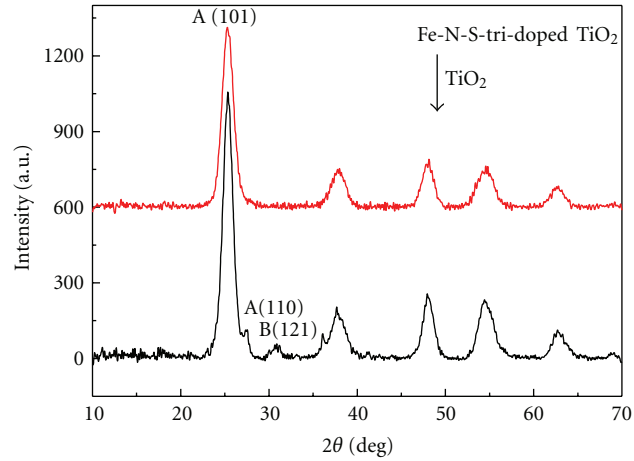

Figure 1: XRD patterns of pure and Fe-N-S-tridoped TiO_2 photocatalysts.

no XRD peaks related to the dopants were detected. One reason was that the concentration of the dopants was so low that it cannot be detected by XRD. The other was that the dopants were incorporated into the lattice of TiO_2 by substituting oxygen and titanium atoms or located in the interstitial sites. Further, the average crystallite sizes of the as-synthesized TiO_2 samples can be calculated by applying the Debye-Scherrer formula [13] on the anatase (101) diffraction peaks. After calculating, the crystallite sizes were found to be 10 and 5 nm for pure and Fe-N-S-tridoped TiO_2, respectively. Thus, we can conclude that tri-doping with Fe, N, and S elements could effectively retard the phase transformation of TiO_2 from anatase to rutile and growth of crystallite sizes.

3.2. XPS Analysis. In order to investigate the chemical states of dopants in Fe-N-S-tridoped TiO_2 photocatalyst, high-resolution XPS of Fe2p, N1s, and S2p were measured and shown in Figure 2. As shown in Figure 2(a), two peaks at 710.9 and 723.9 eV seen from the Fe2p core-level XPS spectrum were assigned to Fe2p3/2 and Fe2p1/2 photoelectrons [14, 15], respectively, demonstrating that Fe was incorporated into the lattice of TiO_2 through substituting the lattice titanium atoms as the form of Fe (III). As seen from Figure 2(b), two peaks at binding energies of 399.6 and 401.6 eV were observed. The first major peak was attributed to the substitutional N in the O-Ti-N structure [10, 16], indicating that some lattice O atoms were substituted by N atoms. The latter peak was attributed to the presence of interstitial N state as the characteristic of Ti-O-N in the doped TiO_2 sample [17, 18]. As seen from Figure 2(c), a single S2p peak located at 168.8 eV was observed, which was attributed to the presence of S^{6+}, suggesting that S was incorporated into the lattice of TiO_2 through substituting titanium atoms [19, 20].

3.3. DRS Analysis. The optical properties of as-synthesized TiO_2 samples were investigated by UV-visible diffuse reflectance spectra and shown in Figure 3. As seen from

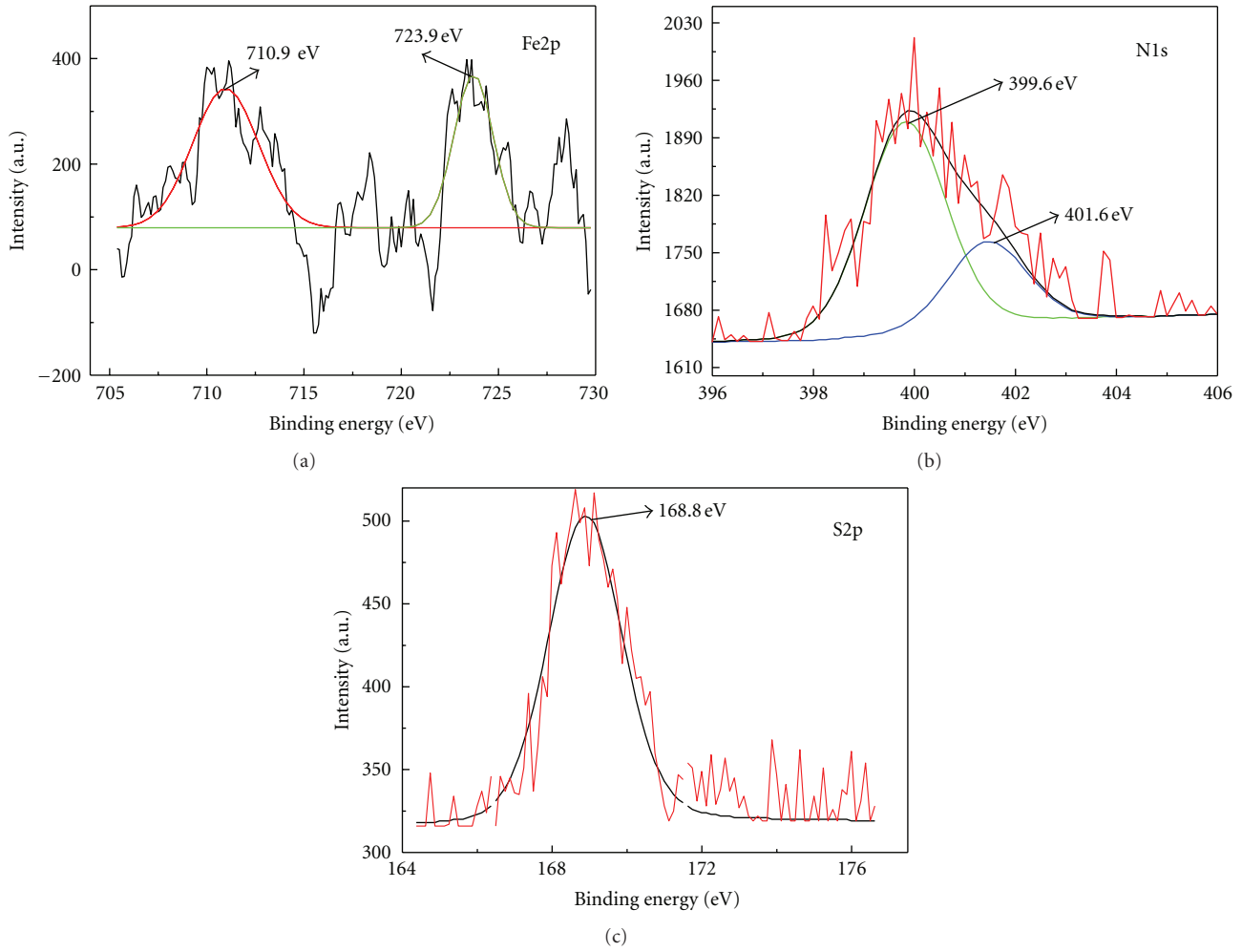

Figure 2: The bind energies of Fe2p (a), N1s (b), and S2p (c) of Fe-N-S-TiO_2 photocatalyst.

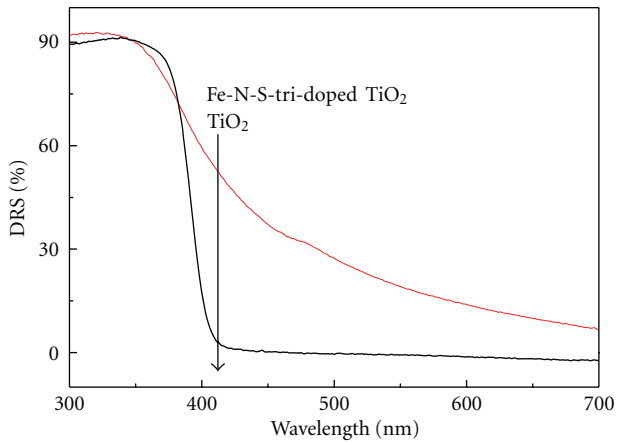

Figure 3: UV-visible DRS of pure and Fe-N-S-tridoped TiO_2 photocatalysts.

Figure 3, in both pure and Fe-N-S-tridoped TiO_2 samples, the onset of absorption edge was observed at 388 nm, corresponding to the band gap energy of 3.20 eV from anatase TiO_2. However, the absorbance edge of Fe-N-S-tridoped TiO_2 was greatly red-shifted to visible light region. As shown in [21], the typical absorbance edge of N-doped TiO_2 was ranged from 380 to 500 nm due to the formation of localized N2p level above the top of valence band edge. Thus, in this study, the enlarged light absorbance in the range of 380~500 nm was attributed to the N doping, while the enhanced absorbance in the range of 500~700 nm was possibly due to the synergistic contribution from the tridoped species. Thus, it is reasonable that the Fe, N, and S elements were indeed incorporated into the lattice of TiO_2, leading to the difference in the crystal and electronic properties of the tridoped TiO_2.

3.4. Photocatalytic Activity. The degradation of phenol was used to evaluate the photocatalytic activities of the as-synthesized TiO_2 samples. The photocatalytic activity of P25 TiO_2 was conducted as a reference. The experimental results were shown in Figure 4. Obviously, as seen from Figure 4, Fe-N-S-tridoped TiO_2 exhibited higher visible light photocatalytic activity than that of pure TiO_2 and P25 TiO_2, for which 85.9% of phenol can be degraded after 2 h of

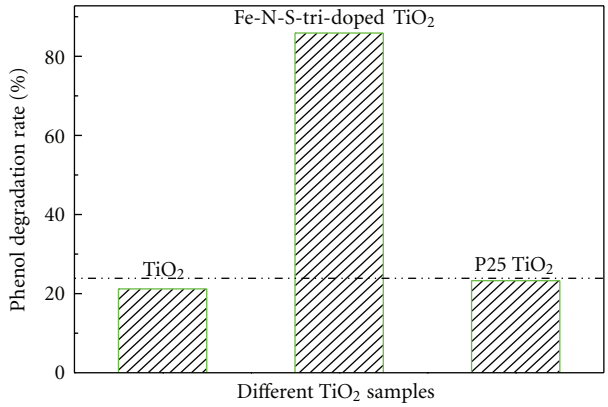

Figure 4: Photocatalytic degradation rate of phenol on different TiO_2 photocatalysts.

visible light irradiation. The enhanced photocatalytic activity was mainly attributed to small crystallite size, intense light absorbance in visible region and narrow band gap energy.

4. Conclusions

In summary, Fe-N-S-tridoped TiO_2 photocatalyst was successfully synthesized by one step in the presence of ammonium ferrous sulfate. Fe (III) and S^{6+} were simultaneously incorporated into the lattice of TiO_2 through substituting titanium atoms, and N might coexist in the forms of substitutional N (N-O-Ti) and interstitial N (O-Ti-N) in tridoped TiO_2. In addition, tri-doping with Fe, N, and S elements could effectively retard the phase transformation of TiO_2 from anatase to rutile and growth of crystallite size. The light absorbance edge of TiO_2 was greatly improved by tri-codoping with Fe, N, and S elements. The as-synthesized Fe-N-S-tridoped TiO_2 presented higher visible light photocatalytic activity for the degradation of phenol than that of pure TiO_2 and P25 TiO_2. The enhanced photocatalytic activity was mainly attributed to the small crystallite size, intense light absorbance in visible region, and narrow band gap energy.

Acknowledgments

The authors wish to gratefully acknowledge the financial support by National Natural Science Foundation of China for Youth (21106035) and Youth Scholar Backbone Supporting Plan Project for general colleges and universities of Heilongjiang province (1151G034).

References

[1] J. H. Carey, J. Lawrence, and H. M. Tosine, "Photodechlorination of PCB's in the presence of titanium dioxide in aqueous suspensions," *Bulletin of Environmental Contamination and Toxicology*, vol. 16, no. 6, pp. 663–668, 1976.

[2] S. K. Joung, T. Amemiya, M. Murabayashi, and K. Itoh, "Relation between photocatalytic activity and preparation conditions for nitrogen-doped visible light-driven TiO_2 photocatalysts," *Chemistry A*, vol. 12, pp. 5526–5534, 2006.

[3] A. Solbrand, A. Henningsson, S. Södergren, H. Lindström, A. Hagfeldt, and S. E. Lindquist, "Charge transport properties in dye-sensitized nanostructured TiO_2 thin film electrodes studied by photoinduced current transients," *Journal of Physical Chemistry B*, vol. 103, no. 7, pp. 1078–1083, 1999.

[4] S. Kohtani, A. Kudo, and T. Sakata, "Spectral sensitization of a TiO_2 semiconductor electrode by CdS microcrystals and its photoelectrochemical properties," *Chemical Physics Letters*, vol. 206, no. 1–4, pp. 166–170, 1993.

[5] M. Bowker, P. Stone, R. Bennett, and N. Perkins, "Formic acid adsorption and decomposition on TiO_2(1 1 0) and on Pd/TiO_2(1 1 0) model catalysts," *Surface Science*, vol. 511, no. 1–3, pp. 435–448, 2002.

[6] R. Asahi, T. Morikawa, T. Ohwaki, K. Aoki, and Y. Taga, "Visible-light photocatalysis in nitrogen-doped titanium oxides," *Science*, vol. 293, no. 5528, pp. 269–271, 2001.

[7] H. Sun, Y. Bai, Y. Cheng, W. Jin, and N. Xu, "Preparation and characterization of visible-light-driven carbon—Sulfur-codoped TiO_2 photocatalysts," *Industrial and Engineering Chemistry Research*, vol. 45, no. 14, pp. 4971–4976, 2006.

[8] K. Lv, H. Zuo, J. Sun et al., "(Bi, C and N) codoped TiO_2 nanoparticles," *Journal of Hazardous Materials*, vol. 161, no. 1, pp. 396–401, 2009.

[9] H. Xu and L. Zhang, "Controllable one-pot synthesis and enhanced visible light photocatalytic activity of tunable C-Cl-Codoped TiO_2 nanocrystals with high surface area," *Journal of Physical Chemistry C*, vol. 114, no. 2, pp. 940–946, 2010.

[10] Y. Cong, J. Zhang, F. Chen, M. Anpo, and D. He, "Preparation, photocatalytic activity, and mechanism of nano-TiO_2 Co-doped with nitrogen and iron (III)," *Journal of Physical Chemistry C*, vol. 111, no. 28, pp. 10618–10623, 2007.

[11] Y. Wang, Y. Huang, W. Ho, L. Zhang, Z. Zou, and S. Lee, "Biomolecule-controlled hydrothermal synthesis of C-N-S-tridoped TiO_2 nanocrystalline photocatalysts for NO removal under simulated solar light irradiation," *Journal of Hazardous Materials*, vol. 169, no. 1–3, pp. 77–87, 2009.

[12] P. Wang, P.-S. Yap, and T.-T. Lim, "C-N-S tridoped TiO_2 for photocatalytic degradation of tetracycline under visible-light irradiation," *Applied Catalysis A*, vol. 399, no. 1-2, pp. 252–261, 2011.

[13] Q. Zhang, L. Gao, and J. Guo, "Effects of calcination on the photocatalytic properties of nanosized TiO_2 powders prepared by $TiCl_4$ hydrolysis," *Applied Catalysis B*, vol. 26, no. 3, pp. 207–215, 2000.

[14] T. K. Ghorai, S. K. Biswas, and P. Pramanik, "Photooxidation of different organic dyes (RB, MO, TB, and BG) using Fe(III)-doped TiO_2 nanophotocatalyst prepared by novel chemical method," *Applied Surface Science*, vol. 254, no. 22, pp. 7498–7504, 2008.

[15] M. Descostes, F. Mercier, N. Thromat, C. Beaucaire, and M. Gautier-Soyer, "Use of XPS in the determination of chemical environment and oxidation state of iron and sulfur samples: constitution of a data basis in binding energies for Fe and S reference compounds and applications to the evidence of surface species of an oxidized pyrite in a carbonate medium," *Applied Surface Science*, vol. 165, no. 4, pp. 288–302, 2000.

[16] J. H. Xu, J. Li, W. L. Dai, Y. Cao, H. Li, and K. Fan, "Simple fabrication of twist-like helix N,S-codoped titania photocatalyst with visible-light response," *Applied Catalysis B*, vol. 79, no. 1, pp. 72–80, 2008.

[17] G. Zhang, X. Ding, F. He et al., "Preparation and photocatalytic properties of TiO_2-montmorillonite doped with nitrogen and sulfur," *Journal of Physics and Chemistry of Solids*, vol. 69, no. 5-6, pp. 1102–1106, 2008.

[18] H. Han and R. Bai, "Buoyant photocatalyst with greatly enhanced visible-light activity prepared through a low temperature hydrothermal method," *Industrial and Engineering Chemistry Research*, vol. 48, no. 6, pp. 2891–2898, 2009.

[19] M. Zhou and J. Yu, "Preparation and enhanced daylight-induced photocatalytic activity of C,N,S-tridoped titanium dioxide powders," *Journal of Hazardous Materials*, vol. 152, no. 3, pp. 1229–1236, 2008.

[20] S. Liu and X. Chen, "A visible light response TiO_2 photocatalyst realized by cationic S-doping and its application for phenol degradation," *Journal of Hazardous Materials*, vol. 152, no. 1, pp. 48–55, 2008.

[21] X. Chen and C. Burda, "The electronic origin of the visible-light absorption properties of C-, N- and S-doped TiO_2 nanomaterials," *Journal of the American Chemical Society*, vol. 130, no. 15, pp. 5018–5019, 2008.